UNIVERSITY
OF TRENTO - Italy
Department of Physics

CONFINDUSTRIA TRENTO

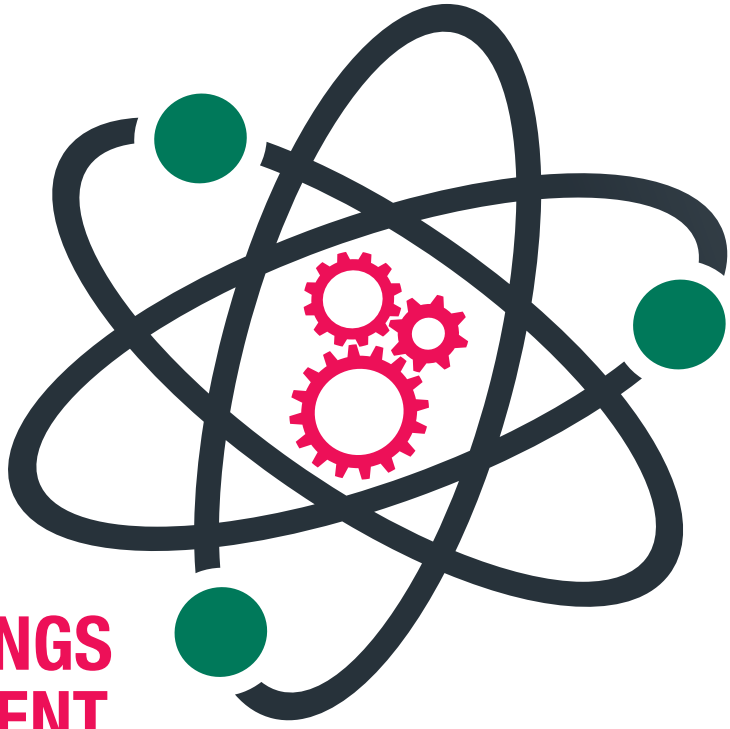

PROCEEDINGS OF THE EVENT

IPSP2014

INDUSTRIAL PROBLEM SOLVING WITH PHYSICS

Trento (Italy)

July 21st – 26th, 2014

UNIVERSITY
OF TRENTO - Italy
Department of Physics

CONFINDUSTRIA TRENTO

Proceedings of the event IPSP2014

Industrial Problem Solving with Physics
Trento, July 21st – 26th, 2014

Editors
Matteo Franchi
Davide Gandolfi
Luca Matteo Martini

Trento
Università degli Studi di Trento

Proceedings of the event IPSP2014: Industrial Problem Solving with Physics: Trento, July 21st - 26th, 2014 / editors Matteo Franchi, Davide Gandolfi, Luca Matteo Martini. - Trento: Università degli Studi di Trento, 2014. - 75 p.: ill. - ISBN: 978-88-8443-581-1.

PREFACE

Dear reader,

thanks for your interest in the first edition of Industrial Problem Solving with Physics. First of all, let us introduce ourselves: we are three PhD. students in Physics from the University of Trento in our last year of studies. We grew up — especially working on the project for the master thesis and during our PhD years — with passion for applied physics: with IPSP2014, we wanted to have the chance to put in practice our experiences and knowledge to real-life industrial R&D. By promoting and realizing this event we had the chance to share this opportunity with other students and researchers that, like us, were motivated and curious to try such experience. The inspiration for the realization of this event came from the well-established Physics with Industry, organized by the FOM Foundation in the Netherlands. This event is held on a yearly basis, and the fifth edition is going to start in these days. We adapted their format to the size of our local community and of the student network of the University of Trento. For the realization of this first edition, we received a great support from the Department of Physics and the Research and Technology Transfer Support of the University of Trento, as well as from Confindustria Trento. They accepted our proposal and, most important, they believed in us. Their support has been a major motivation to invest our time and our efforts in the organization of the workshop, and for this we are really grateful to them. Another big satisfaction and reward for our work came from the feedback of the students and of the companies. As regards students/researchers, even if we received less applications than the available positions, the selected applicants participated with passion, and worked as a team by forming several groups that tackled the problems from multiple perspectives. Also the participation to social events was a good proof of their engagement. The positive feedback of the companies was shown by the high number of applications that we received and proven by the appreciation of the participating ones. This is a clear indication that in the Trentino area there are many highly-technological companies that feel the need for innovation and are willing to invest in research. At the same time, however, a career in a company is not perceived by many students as a valuable alternative to the academic one. Our

hope is that the feedback from participants of this edition will work as a catalyst for rising students awareness and attracting their interest for future editions of IPSP. Lastly, a major and unexpected outcame of this workshop is the big impact of the solutions found by the young researchers: a commission for the realization of a diagnostic system to be installed in the R&D line, a couple of research projects that are under definition and one idea currently under investigation for patent filing.

Matteo Franchi
Davide Gandolfi
Luca Matteo Martini
Scientific Committee of Industrial Problem Solving with Physics 2014

INTRODUCTION

Industrial Problem Solving with Physics 2014 (IPSP2014) is a one-week-long workshop organized by the Department of Physics of the University of Trento, in collaboration with the local industrial organization, Confindustria Trento, and the Research and Technology Transfer Support of the University of Trento. This event took place from the 21st to the 26th of July, 2014, in Trento, Italy.

The aim of the workshop was to allow young and motivated university students/researchers to apply their knowledge and skills to solving industrial problems. This experience gave them the opportunity to display their talent, in view of future collaborations or job careers. In addition, it has been a great opportunity to strengthen the technological know-how and human resources exchange between the academic system, in particular the Department of Physics, and companies. By participating to the event, in fact, the companies received solutions to their problems and experienced a new approach to research and development.

The participation to the event has been restricted only to three industrial companies and to 30 students/researchers, which were selected by means of a call available on the official website `http://events.unitn.it/en/ipsp2014`. Considering that this was just the first edition organized by the University of Trento, the response of the companies to the call has been really positive: the committee for the selection of the applications received 8 industrial problems, all of them qualified and very interesting. As far as students are concerned, the response was not as impressive: we received 24 eligible applications. During the working sessions, the young researchers were grouped by their affinity to the problems and by their knowledge background. After a quick introduction to the companies profiles and to the problems, the groups started working in close collaboration with the industrial partners. This cooperation has been fundamental for reaching quickly the "state-of-the-art", and to wisely choose new investigation methods. The research activities have been focused on literature readings, computer simulations, theoretical modelling and laboratory experimental investigation. At the end of the week the groups summarized all the collected materials to present their solutions to the other participants and to the proposing company.

All the solutions proposed by the researchers were judged positively by the

industrial partners, both in terms of effectiveness and novelty. This result was confirmed also by the plans of further research and development that have been commissioned to the Department of Physics after the event. Lastly, some ideas proposed are currently under investigation for patent filing.

The present document is structured as follows: the first chapter is about the problem of Adige S.p.A., the second is dedicated to the problem proposed by Aquafil S.p.A. and the last one for the problem of Röchling Automotive SE & Co. KG. All the chapters contain a section dedicated to the presentation of the problem, followed by the description of the investigation and finally by the summary of the results.

CHAPTER

ONE

METHODS AND INSTRUMENTATION FOR THE STUDY OF THE FLUID DYNAMICS OF THE ASSIST GAS DURING LASER CUTTING

M. Bernard, C. Castellan, S. Donadello, M. Eccher, M. Mancinelli, M. Scapinello, A. Toffali, A. Trenti

Abstract

Adige S.p.A. is a world leader company in projecting, producing and selling lasertube cutting systems. Two different systems are available, one based on fusion and the other on oxidation of the material that has to be cut. Both these techniques require the presence of a laser beam well focalised on the material and an assistance gas stream, used to eject the melted material. Until now paths for gas injection and in particular nozzles are drawn using empirical criteria, based on cutting tests. The idea of this work is to find some experimental techniques able to correlate the design of the gas path to the process performance. In addition to this, experimental measurements will be useful to validate numerical simulations of the process. The idea is trying to design and validate an experimental apparatus able to measure the pressure (or the velocity) of the gas during its path across the machine, both inside and outside the nozzle.

1.1 Introduction

During IPSP2014, different techniques have been proposed. Here they are listed and briefly described, emphasising in particular their main positive and negative aspects.

1.1.1 Hot-wire anemometers

Hot-wire anemometry is one of the most used invasive techniques. It has the great advantage of being directly available on the market, and it is portable and

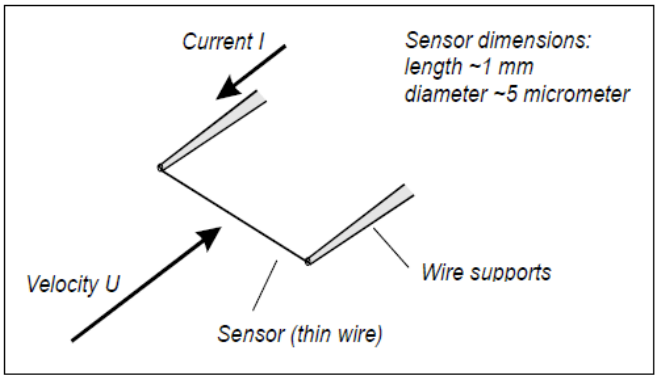

Figure 1.1: Structure for an hot wire anemometer.

can be used also on industrial machines, not only in the laboratory scale. The disadvantages of this technique is that hot-wire anemometers are invasive and so the measured quantity can be affected by systematic errors. Anyway, the use of this technique could be very interesting to monitor the proper functioning of the machinery (also made by technicians in the place where the system is operating).

Hot wire anemometers use a very thin wire, which is electrically heated up to a temperature above the ambient one. The measurement technique is based on the heat transfer from the metal wire to the relatively cold gas flowing over the wire.

The wire material is typically platinum or tungsten, which is $1 \div 10\,\mu\text{m}$ in diameter and about 1 mm in length. A schematic representation of the apparatus is given in Figure 1.1. The heat dissipated by the wire is a function of the gas velocity. Using fluid dynamic equations, a relationship between the fluid velocity and the electrical output of the system can be established.

Description of the hot-wire anemometer measurement

Let us consider a wire that is immersed in a fluid flow. Assume that the wire, heated by an electrical current input, is in thermal equilibrium with its environment. The electrical power input is equal to the power lost to convective heat transfer, that is:

$$I^2 R_W = h A_W (T_W - T_f)$$

where I is the input current, R_W is the resistance of the wire, T_W and T_f are the temperatures of the wire and fluid respectively, A_W is the projected wire surface area, and h is the heat transfer coefficient of the wire. This is a good approximation for $T_W < 1000\,\text{K}$ and fluid velocity larger than $0.2\,\text{m}\,\text{s}^{-1}$ [1].

The wire resistance R_W is also a function of temperature according to:

$$R_W = R_{ref}[1 + \alpha(T_W - T_{ref})]$$

where α is the thermal coefficient of resistance and R_{ref} is the resistance at the reference temperature T_{ref}.

The heat transfer coefficient h is a function of fluid velocity v_f according to King's law,

$$h = a + bv_f^c$$

where a, b, and c are obtained from calibration ($c \simeq 0.5$).

Combining the above three equations allows us to eliminate the heat transfer coefficient h,

$$a + bv_f^c = \frac{I^2 R_w}{A_W(T_W - T_f)} = \frac{I^2 R_{ref}[1 + \alpha(T_W - T_{ref})]}{A_W(T_W - T_f)}$$

. We can solve for the fluid velocity,

$$v_f = \left[\left[\frac{I^2 R_{ref}[1 + \alpha(T_W - T_{ref})]}{A_W(T_W - T_f)} - a\right]\frac{1}{b}\right]^{(1/c)}$$

.

The hot-wire anemometer operates in two regimes, a constant-current (CC) regime ($I_W = const$) when the gauge voltage pulsations are attributable to temperature variation and, hence, the wire resistance, and a temperature constant (CT) regime ($T_W = const$), maintained by the feedback system with a variable current heating the sensor. The amount of energy lost can be calculated from the temperature change in the constant current case, or the current change in the constant temperature change. Constant-temperature anemometers are more widely used than constant-current anemometers due to their larger dynamic range. When $T_W = cost$, the fluid velocity is a function of input current and flow temperature only. The gauge wire is connected by a shielded coaxial cable to one of the arms of Wheatstone bridge, the opposite arm being connected to a variable resistance controlling the overheat factor $m = R_W/R_C$. In CT a feedback amplifier controls the bridge current so as not to upset the bridge balance and, consequently, to retain the gauge resistance and temperature constant and independent of the cooling rate. The instantaneous unbalanced voltage of the bridge determines an instantaneous value of velocity pulsation. Nowadays instrument circuits afford, at an optimal alignment, a bandwidth up to hundreds of kHz.

Example of a commercially available hot wire anemometer

Dantec Dynamics offers a complete probe system for use with Constant Temperature Anemometers (CTA). Miniature wire probes have 5 µm diameter, 1.25 mm long platinum-plated tungsten wire sensors. The wires are welded directly to the prongs and the entire wire length acts as a sensor. The probe body is a 1.9 mm diameter ceramic tube, equipped with gold-plated connector pins that connect to the probe supports by means of plug-and-socket arrangements. These probes are general purpose probes recommended for most measurements in one-dimensional flows. They measure mean flow velocities and fluctuations. One of the available probes (miniature probe category) is the product 55P14, represented

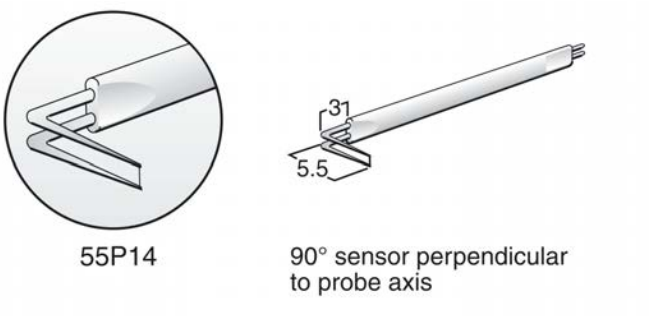

Figure 1.2: On the left, a schematic of 55P14 anemometer. On the right, the same anemometer is reported perpendicular to probe axis [2].

in Figure 1.2, having right-angled prongs with the sensor perpendicular to probe axis. This configuration makes this probe suitable for boundary layer measurements, e.g. in pipes, as well. These probes can measure flux velocities up to the supersonic regime ($500\,\mathrm{m\,s^{-1}}$) and have a flat frequency response ($< 3\,\mathrm{dB}$) up to 400 kHz in CTA mode.

Table 1.1: Technical Data For Miniature Wire Sensors.

Medium	Air
Sensor material	Platinum-plated tungsten
Sensor dimensions	5 µm dia, 1.25 mm long
Sensor resistance R20 (approx)	3.5
Temperature coefficient of resistance (TCR) α 20 (approx.)	$0.0036\,^{\circ}\mathrm{C}^{-1}$
Max. sensor temperature	300 °C
Max. ambient temperature	150 °C
Max. ambient pressure	Depends on the type of mounting
Min. velocity	$0.05\,\mathrm{m\,s^{-1}}$
Max. velocity	$500\,\mathrm{m\,s^{-1}}$
Frequency limit fcpo (CCA mode, $0\,\mathrm{m\,s^{-1}}$)	90 Hz
Frequency limit fmax (CTA mode)	400 kHz

Given its dimensions and shape, probe 55P14 seems to be a good option to evaluate the gas flow output of typical nozzles used in laser cutting technologies. Lets consider z-axis as the main axis of a nozzle (coincident to laser beam direction), having an aperture diameter of 1 mm. Moving the probe within a plane, at a certain distance from the nozzle exit, does not provide good resolution 2D ($x-y$ plane) mapping of the flux velocities, since each measure refers to the entire length of the wire (1.25 mm). Probably a rough distribution of velocities could be reconstructed by assuming a Gaussian shape of the flux. The measurements can be used anyhow to evaluate the transversal dimension of the gas flow. This can

easily be done at every z value, allowing to understand how the flux varies as a function of the nozzle standoff (typical standoff lower than 1 mm for this nozzle size). For a bigger nozzle (3 mm aperture), more acquisition points would contribute to evaluate the flux distribution. Alternatively, bigger probes can be used. By placing the probe on top of the workpiece, along the cut line, an estimation of the mean flux during the laser-cutting operation can be obtained. Another type of evaluation is the fluctuation of the flow due to the high-frequency response of the probe.

Feasibility and cost

The potential benefits from an apparatus based on hot wire anemometry have already been presented. Some uncertainties about the robustness of such a system remain. The small dimension of a miniature probe is a great advantage, since it is expected not to significantly change the flow characteristics; on the other hand it is not clear whether this system will hold out against high flux conditions. One of the main issue to face in order to have a quantitative evaluation of the gas flow is the calibration of the probe for the convective heat transfer to nitrogen, which is used as assist-gas in the cutting-machine by Adige S.p.A. Some works can be found in literature about the calibration procedure. A limitation for these devices is the requirement for frequent calibration if contamination occurs over time.

An in-situ apparatus for hot wire anemometry is composed by four basic component: a measuring-system frame with micrometric adjustment, electronic instrumentation (a digital multimeter and a power supply), a hot wire probe and a Wheatstone bridge circuit. If the frame and the electronic instrumentation are already part of the company equipment, the purchase reduces to the probe and to the circuitry.

1.1.2 Doppler shift - LDA

Optical techniques allow the measurement of the local and instantaneous velocity of tracer particles to be done while not disturbing the carrier flow. In particular we can apply the familiar concept of Doppler shift to fluid mechanics: when light is reflected from a moving object, the frequency of the scattered light is shifted by an amount proportional to the speed of the object. On the other hand, the object speed can be estimated by measuring the light frequency shift.

If the flow is seeded with small, neutral particles that scatter light, which are illuminated by a known laser light frequency. The difference between the incident and scattered light frequencies is called the *Doppler shift* $\Delta\nu$. It is described by the relation [3]

$$\Delta\nu = \frac{2v}{\lambda}\cos\beta\sin\frac{\alpha}{2},$$

where v denotes the particle velocity, λ the wavelength of the light, α and β refer to Figure 1.3. By scanning the flow we can map the velocity of the tracer particles averaging along the laser beam.

Laser Doppler anemometry (LDA) represents an improvement of this technique, in which the laser beam from the source is split into two parts that cross to

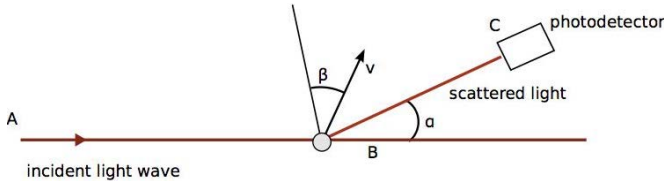

Figure 1.3: A particle moving through an incident light wave of frequency ν scatters light in all directions. Scattered light picked up by the photodetector will be shifted by $\Delta\nu$. α is the angle between the incident light wave and the photodetector, β denotes the angle between the velocity vector and the bisector of ABC.

provide an interference pattern in the local region of flow where velocity measurement is required [4]. As a particle crosses the fringe pattern, the intensity of the scattered light is modulated with the intensity of the fringes (Figure 1.4). The frequency of the amplitude modulation is the Doppler frequency $\Delta\nu$.

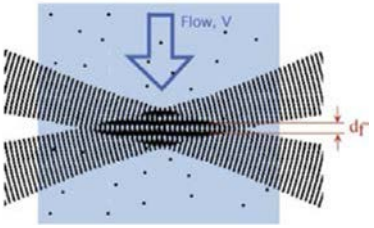

Figure 1.4: A fringe pattern is created at the intersection of the two incident beams, with fringe spacing d_f. The frequency of the modulation gives the Doppler frequency $\Delta\nu = v/d_f$.

Feasibility and cost

Doppler shift and LDA are techniques typical of research laboratories. These setups are not commercially available, due to the complexities related to the development and the use of these techniques, but they can be made custom. University, research institutes and specialised companies (e.g. Dantec Dynamics) could offer the possibility to develop the best custom system related to the problem. The cost is generally high compared to other commercially available products, but these techniques aren't invasive and they are more accurate. Coupling Doppler shift and LDA with a transparent section of the cutting head, makes it possible to map the velocity of the fluid inside the chamber.

1.1.3 Acoustic interferometry

Since the 19th century rudimentary acoustic antennas consisting of simple horns were used to locate ships in the fog. This method was improved during World War

I to detect enemy aircrafts, but experienced a stop later on due to the development of radar technology. Nowadays acoustic interferometry is a widely-used technique in the field of imaging noise inside mechanical parts and machinery.

It makes use of array antennas of microphones to sense sound (pressure waves) with a high spatial precision. Since this method is based on the interference of the sound waves at different positions, the spatial distribution of the microphones is a crucial parameter along with the wavelength that is employed. Hence we tried to design an experiment for measuring pressure with acoustic interferometry, and we performed some Finite Elements Method simulations (FEM).

We simulated a circular antenna searching for the optimal number and positions for the microphones and possible further elements such as a reflector, in order to maximise the signal-to-noise ratio and spatial resolution.

Nevertheless microphones available in our laboratory allow us to obtain an insufficient spatial resolution, of about 1 cm, mainly due to their bandwidth, which is limited to 15 kHz. Therefore we made a market research finding out two main categories of detectors.

The first is the proper acoustic antenna, which makes a 2D image, exactly as a camera. Hence the resolution of such a method is in the range of $1 \div 5$ degrees.

The second one is a 3D imaging technique, which allows a three-dimensional tomography of the sample.

Feasibility and cost

Although this technique could, in principle, give us 3D maps of gas flow and pressure and could give information even in the kerf, the realisation complexity, low spatial resolution and difficult calibration analysis make acoustic interferometry not suitable for this application.

1.1.4 Schlieren photography

Schlieren photography is an imaging system that uses optical techniques for the visualisation of density gradients inside a fluid. This method has been developed in 19th century, and is essentially interested in giving a visual study of what is happening. It is often used to study the dynamics of a fluid. Schlieren photography is based on the principle that, if the refractive index of a medium is changed, the path of the light that passes through that material is modified [5]. In order to take advantage of this mechanism, a light source illuminates the analysed region and its image is observed on a screen. A brief scheme of the apparatus is given in Figures 1.6 and 1.7. A knife edge is placed between the probe and the screen in order to stop one half of the image (Figure 1.5). In that way:

- if there are no changes in the density gradient, the knife simply darkens the image;
- if there is a variation of the density gradient inside the probe, this induces a variation in the propagation direction of the light beams inside the probe; it could happen that some beams that were blocked without the probe now

are visible, and on the other side some beams visible without the probe can be now invisible on the screen; in this way a sharp contrast in the image is induced.

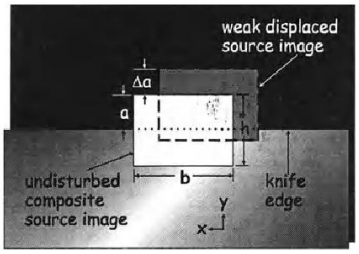

Figure 1.5: Diagram of tangential focus in a z-type schlieren system, showing horizontal smearing of the light-source image and the proper application of a horizontal knife-edge cutoff [5].

Theoretical background

Light propagates uniformly through media, but disturbances and inhomogeneities can change the media density and with it the refractive index. This can cause the rays of light travelling through media to bent. For example for air there is a simple relationship between the refractive index and the gas density ρ:

$$n - 1 = k\rho,$$

k is the Gladstone-Dale coefficient, that for air is about $0.23\,\mathrm{cm}^3\,\mathrm{g}^{-1}$. The refractive index is only weakly dependent upon ρ, and, as the refractivity $n - 1$ of a gas, depends upon the gas composition, temperature, density and wavelength. The bending or refraction of light rays can be understood using geometrical optics. Let's take a Cartesian x,y,z system. Suppose that the light travels along the z-direction. It can be demonstrated that the light rays are refracted by optical inhomogeneities in proportion to the gradient of the refractive index in the x,y-plane. The resulting ray curvature is given by:

$$\frac{\partial^2 x}{\partial z^2} = \frac{1}{n}\frac{\partial n}{\partial x} \qquad \frac{\partial^2 y}{\partial z^2} = \frac{1}{n}\frac{\partial n}{\partial y},$$

integrating once we obtain:

$$\epsilon_x = \frac{1}{n}\int \frac{\partial n}{\partial x}\partial z \qquad \epsilon_y = \frac{1}{n}\int \frac{\partial n}{\partial y}\partial z,$$

for a two-dimensional schlieren of extent L along z-axis, this becomes:

$$\epsilon_x = \frac{L}{n_0}\int \frac{\partial n}{\partial x} \qquad \epsilon_y = \frac{L}{n_0}\int \frac{\partial n}{\partial y},$$

where n_0 is the refractive index of the surrounding medium. These relations are the basis for the mathematical modelling of this technique.

Experimental setup

The most used schlieren setup is the Toepler's one, characterised by the presence of the slit-source and the knife-edge to partially cutoff the light before the detector. We are going to present the two most used types of Toepler's schlieren schemes. The first one is the dual-field-lens system shown in Figure 1.6. The light coming through an extended non-coherent light source must have at least one edge sharply limited by an opaque mask or knife (a slit in Figures 1.6 and 1.7). Field lens 1 and

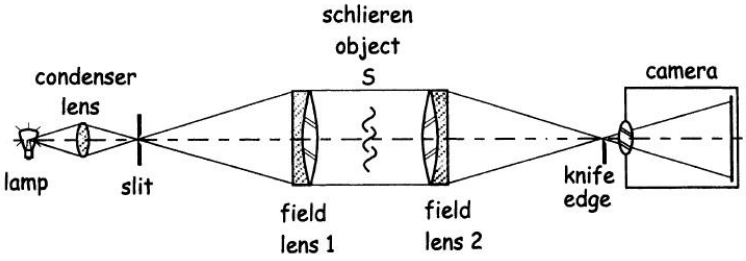

Figure 1.6: Schematic representation of a in-line schlieren set-up [5]

2 cause the light ray to travel parallel inside the test area, and to focus the slit image in the knife-edge plane. The second system is the z-type mirror one. Two opposite tilted on-axis parabolic mirrors (Figure 1.7) illuminate the sample with a parallel beam coming from a divergent light source. The light is then focused on the knife-edge plane. Optics arrangement suggest the letter z, that gives the name to this kind of set-up.

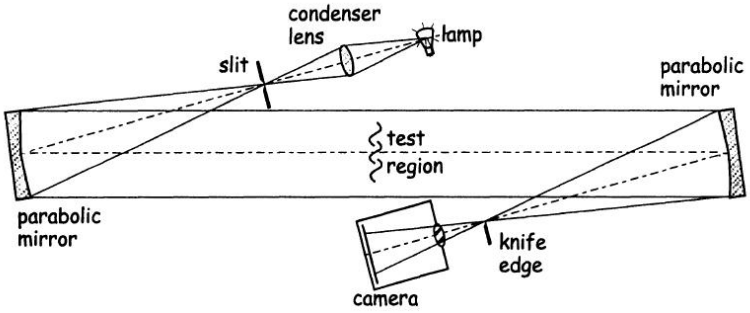

Figure 1.7: Schematic representation of a Z-type schlieren set-up [5]

Sensitivity

Consider a z-type schlieren arrangement (Figure 1.7), with a horizontal source slit orientation and a horizontal knife edge. Given the luminance B of the light

source (in $\mathrm{cd\,m^{-2}}$), the illuminance E_0 incident upon the first mirror is:

$$E_0 = \frac{Bbh}{f_1^2},$$

where b and h are the slit breadth and height, respectively and f_1 the focal length of the first mirror. The schlieren image illuminance is the same of the first mirror, but multiplied by a factor m that takes into account the image size relative to the total test area:

$$E_0 = \frac{Bbh}{m^2 f_1^2}. \tag{1.1}$$

The knife-edge has the function of blocking a fraction of the incoming light at the second mirror focus. Assume that the height of the transmitted light is a, we can replace h in Eq: 1.1 with $a\frac{f_1}{f_2}$:

$$E = \frac{Bba}{m^2 f_1 f_2},$$

that is the background illuminance. If we put a schlieren object in the test area that refracts a certain light ray with an angle $\bar{\epsilon}$ with a the y-component ϵ_y a fraction of source image is shifted upward in the knife-edge plane by a distance $\Delta a = \epsilon_y f_2$. The incremental gain (or differential gain) of the corresponding image point caused by the refraction ϵ_y in the test area is:

$$\Delta E = \frac{Bb\epsilon_y}{m^2 f_1}.$$

We define the contrast C as the ratio of the differential gain to the image background:

$$C = \frac{\Delta E}{E} = \frac{f_2 \epsilon_y}{a}, \tag{1.2}$$

and, finally, the schlieren sensitivity S as the change in image contrast respect to the refraction angle:

$$S = \frac{\partial C}{\partial \epsilon_y} = \frac{f_2}{a}. \tag{1.3}$$

Feasibility and cost

Schlieren photography is an imaging technique typical of research laboratories. This apparatus is not completely commercially available, but it can be made custom. University, research institutes or specialised companies could offer the possibility to develop the best custom system related to the problem. The cost for the material needed for the construction of an apparatus similar to the one presented during the IPSP week is around $5000 - 10000$ €.

1.1.5 Optical fibers

Optical fiber-based devices can be used to measure pressure and velocity field inside and outside the laser-cutting machine head [6]. A typical scheme of an optical fiber with a micro-machined head and its readout apparatus is presented in Figure 1.8. The optical fiber ends with two mirrors that create an optical

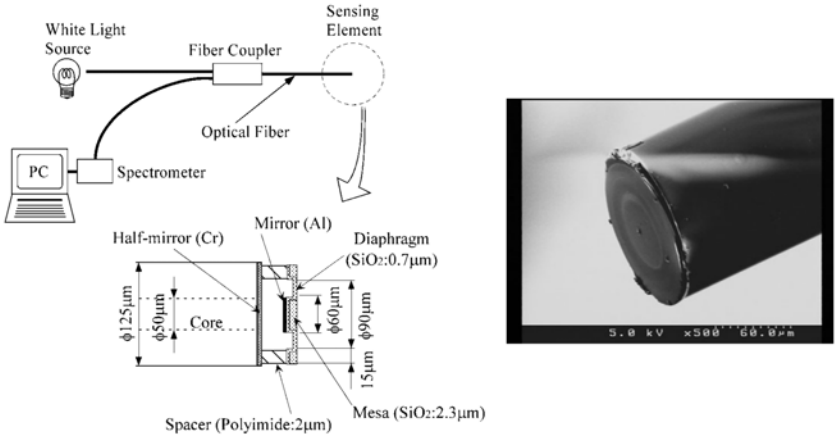

Figure 1.8: Left: scheme of the micro-machined head and read out setup. Right: SEM image of the micro-machined head [6].

cavity called FabryProt interferometer (Figure 1.8) [7]. The suspended mirror (diaphragm) is able to deform under an external pressure thus changing the cavity length. Different cavity lengths correspond to a different spectral response of the optical fiber. The spectral response of the sensing head can be recognised using a white light source and a spectrometer as illustrated in Figure 1.8.

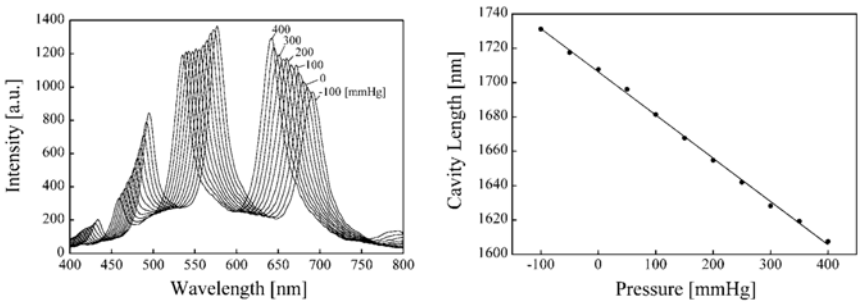

Figure 1.9: Left: spectral response of the sensor for several pressures. Right: sensor calibration curve [6].

Figure 1.9 left shows the spectrum of the sensor for several external pressures. Starting from the previous graph the calibration curve (cavity length vs Pressure)

can be extracted (Figure 1.9 right). The sensor pressure range and the sensitivity can be tuned by changing the diaphragm thickness. This sensor can be applied

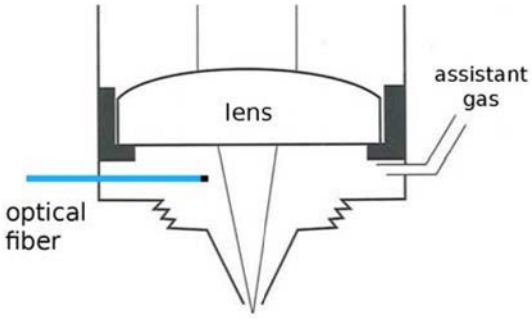

Figure 1.10: Fiber-based pressure sensor inside the chamber.

to map the pressure inside the nozzle and the chamber prior to the nozzle as sketched in Figure 1.10.

Feasibility and cost

Optical fiber-based devices are not commercially available. Universities, research institutes or specialised companies could offer the possibility to develop the best apparatus related to the problem. The cost for the material needed for the construction of an apparatus is in the order of 5000 €.

1.1.6 Strain gauges

A strain gauge is an instrument that measures strains by employing the fact that a mechanical stress on a conductor changes its resistance. More in detail, if we consider a material characterised by a length L and a section $S = W \cdot H$ and subjected to a force F along L, we can define the *stress* as $N = F/S$, and the *strain* as $\varepsilon = \Delta L/L$ [8]. In an elastic regime the strain is proportional to the stress, $\varepsilon = N/E$, with E the Young modulus. A useful parameter characterising a material is the ratio of transverse to axial strain (*Poisson's ratio*):

$$\nu = -\frac{\Delta W/W}{\Delta L/L} = -\frac{\Delta H/H}{\Delta L/L}. \tag{1.4}$$

The resistance of a conductor is described by the law

$$R = \rho L/S, \tag{1.5}$$

where ρ is the material resistivity. Rearranging Eq: 1.5, the ratio between the variation of resistance and the resistance can be expressed as function of the *Poisson's*

ratio Eq: 1.4 and the variation of length $\frac{\Delta L}{L}$ and the variation of resistivity $\frac{\Delta \rho}{\rho}$ can be found:

$$\frac{\Delta R}{R} = (1 + 2\nu)\frac{\Delta L}{L} + \frac{\Delta \rho}{\rho}.$$

The most general case accounts for piezoelectricity of the material, in which $\rho = \rho_0(1 + \beta N)$, with β piezoelectric coefficient. In this case the relative variation of resistance becomes $\Delta R/R = \Delta L/L(1 + 2\nu + \beta E)$. Hence a strain gauge converts a relative length variation into a relative resistance variation. It is characterised by the so-called *Gauge Factor*:

$$G = \frac{\Delta R/R}{\Delta L/L}.$$

Feasibility and cost

A strain gauge-based instrument can be made easily with commercially available systems (strain gauges elements and read out electronics). University, research institute or specialised companies could offer the possibility to develop the best apparatus related to the problem. The cost for the material needed for the construction of an apparatus is in the order of 2000 €.

1.1.7 Comparison between techniques

A brief comparison between the analyzed techniques is reported in Table 1.2.

Table 1.2: Comparison between the analysed techniques.

Technique	Advantages	Drawbacks	Cost
Hot wire anemometer *Flow velocity*	Spatial resolution, high frequency response, in situ, commercially available	Intrusive, necessity of calibration, probe breakage	Low-Medium
Doppler shift-LDA *Flow velocity*	3D mapping, spatial resolution, sensitivity, internal analysis, kerf analysis	Complex equipment, laboratory system	Very high
Acoustic interferometry *Flow pressure*	3D mapping, kerf analysis	Low spatial resolution, complex, difficult calibration	High
Schlieren photography *Flow densitiy*	Real-time imaging, 2D sensitive, kerf analysis, data for modeling	Phenomenological, non-quantitative	Medium
Optical fibers *Flow pressure*	Internal analysis, portable, ease of measurement	Average measures, difficult calibration	Low

Because of the short time available, it has been decided to implement only three of the techniques described up to now, that are:

- schlieren photography;
- optical fibers;
- strain gauges.

These techniques have been considered the most interesting for the solution of problems introduced by Adige S.p.A. They are based on very different approaches, and allow to obtain measurements in different situations. For example, measurements made by optical fibers are the only ones that can give a measurement both inside and outside the nozzle, but their implementation and calibration can be considered more difficult that the measurement made by strain gauges. On the other hand, using strain gauges one can obtain only mean measurements of the pressure inside of the chamber, and nothing about what happens outside. Schlieren photography can be considered very interesting because it can give an immediate visual idea of what is happening, but it is only a qualitative technique and it is difficult to infer absolute values.

In following sections, a more detailed description of the considered techniques is given.

1.2 Schlieren photography

In the following sections we are going to describe our schlieren photography apparatus.

1.2.1 Set-up

We chosen an hybrid set-up between the dual-field-lens and the z-type (Figure 1.11). The light coming through a 3 W-white led was focused by a $f = 50\,\text{mm}$ lens on the slit. The light was then collimated with a $f = 100\,\text{mm}$ lens, then the first mirror (flat, $2''$ diameter) illuminated the sample. The light was then collected and focused on the focal plane of the knife by a circular $f = 200\,\text{mm}$, $2''$ mirror. Finally a $f = 50\,\text{mm}$ lens focused the schlieren image on the CCD (Imaging Source, DMK41AU0.AS) sensor plane. We used the circular mirror in the detector arm to maximise f_2, in order to increase the contrast and the schlieren sensitivity (C and S, respectively, see Eq: 1.2 and Eq: 1.3). The CCD images were recorded and stored by using a program written in LabVIEW that automatically subtracts the background to the sampled images. A Matlab script was used to post process and to increase the contrast of the images. A Phyton script was used for videos post processing.

1.2.2 Results

The set-up was used to characterise a nozzle of 1 mm exit bore (Figure 1.17 left), in function of the pressure applied to the gas feed (Figure 1.12). The gas used

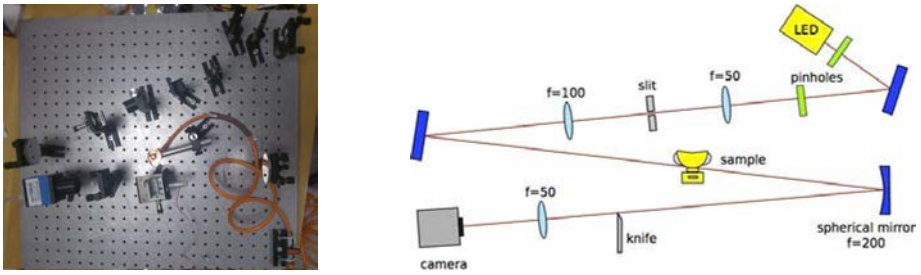

Figure 1.11: Left: realised experimental set-up. Right: Schematic representation of the schlieren apparatus.

was air at room temperature with a pressure range from 1.0 bar to 6.0 bar.

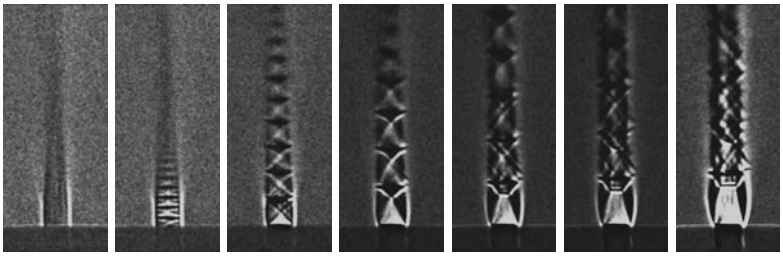

(a) 1.0 bar **(b)** 1.5 bar **(c)** 2.0 bar **(d)** 3.0 bar **(e)** 4.0 bar **(f)** 5.0 bar **(g)** 6.0 bar

Figure 1.12: Evolution of the schlieren image in the test-range (1.0 to 6.0 bar)

We also verified if our apparatus could give good image even if an obstacle is present in the test area. In Figure 1.13 we put vertically a 1″ CaF_2 window over the nozzle, which was fed with 5 bar of air.

In Figures 1.12 and 1.13 are clearly visible regions where the pressure and the velocity of the air exiting from the nozzle are inhomogeneous. The formation of standing wave patterns, that appear increasing the pressure of the gas feed, indicates the presence of shock diamonds (also known as Mach disks). These images should be used to infer crucial information about the fluid-dynamics of the nozzle and can be used to verify theoretical models.

1.3 Optical fibers

In the following sections we are going to describe the development of a novel technique for velocity field measurements inside the cutting-head chamber.

1.3.1 Set-up

The features of an optical fiber-based sensor are:

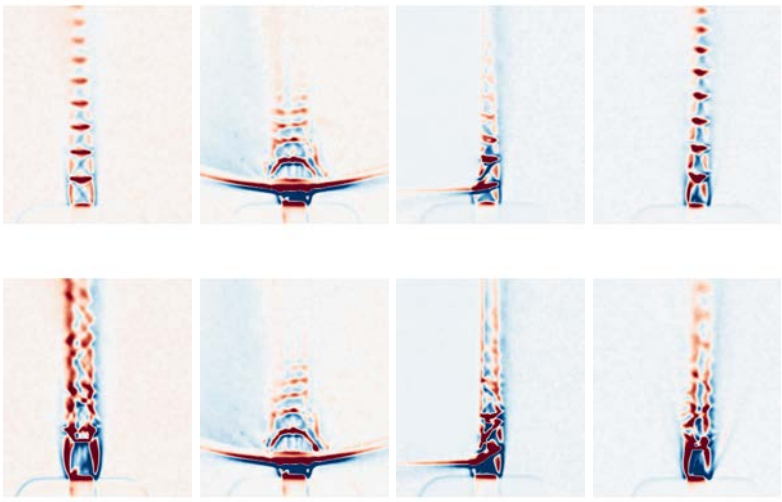

(e) no obstacle **(f)** obstacle front view **(g)** obstacle lateral view **(h)** damaged nozzle

Figure 1.13: Schlieren images of the nozzle bore.

- deformability;
- spatial resolution up to 5 mm;
- sensitive to direction;
- low-cost.

The sensor is a brand new idea developed during the IPSP week. Here is reported just an introduction to the sensor because the idea is going to be patented by the University of Trento. The optical fiber is used as a flux sensor and needs to be placed inside the chamber. In the presence of a gas flux, the fiber sensor will alter the polarization state of the light, because the fiber can feel the flux thanks to the drag force [9]. By looking at the polarization state at the output of the sensor, it is possible to get information on the flux magnitude and on the flux direction.

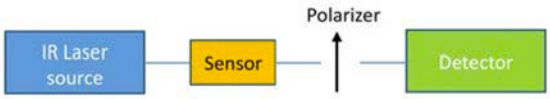

Figure 1.14: Read out set-up

1.3.2 Results

Since we did not have a calibrated flux source, the sensor was calibrated knowing the pressure at the chamber entrance. The pressure range was chosen to have a N_2 flux of the same order of magnitude to that inside the Adige S.p.A. machine. The flux magnitude was estimated using the Bernulli equation. An homemade brass chamber was fabricated to simulate the chamber prior to the nozzle. The experiment was realised under these conditions:

- Input pressure: from 0 to 6 bar;
- Approximate flux $100\,\mathrm{L\,min^{-1}}$;
- Reynolds number > 6000 (turbolent regime);
- Drag force on the fiber $\simeq \mu$N.

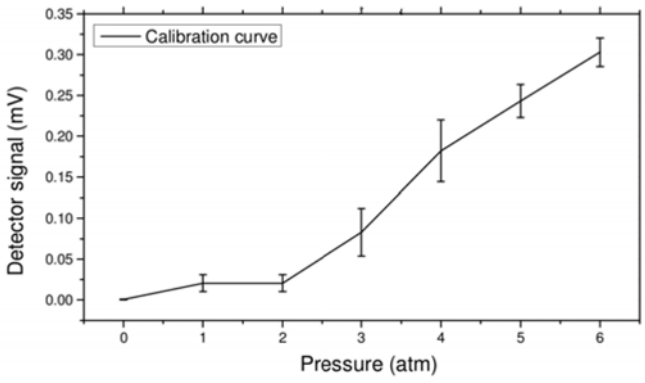

Figure 1.15: Sensor calibration curve. The pressure scale can be seen as the flux magnitude.

Figure 1.15 shows the sensor calibration curve. It is important to remark that a proper calibration would require a gas-flow meter.

1.4 Strain gauges

In the following sections we are going to describe our attempt to realise a strain gauge-based sensor.

1.4.1 Numerical simulation

We perform a FEM numerical simulation using the software COMSOL Multiphysics. We simulate the strain of the nozzle caused by a 20 bar pressure. We suppose that the only mechanical constrain is along the mechanical seal. The pressure at the exit and around the body of the nozzle is 1 bar. The results are shown in

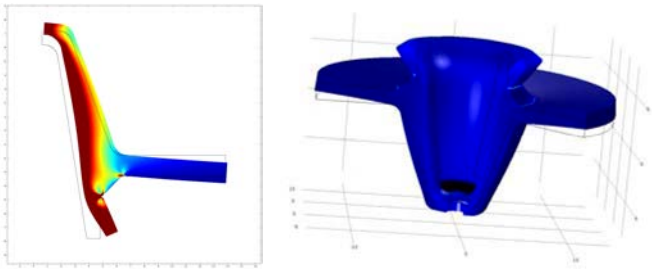

Figure 1.16: Numerical simulation of the nozzle deformation at 20 bar. The deformation is magnified by a factor of 10^3.

Figure 1.16. The maximum estimated strain of the nozzle body is $\Delta L \approx 1\,\mu\text{m}$ at $P = 20\,\text{bar}$.

1.4.2 Set-up

A copper nozzle can be deformed by the gas pressure acting on it. A strain gauge attached on the nozzle body can detect such deformations and, via a proper calibration, it can return an estimation of the pressure value. In our test apparatus we used a Micro-Measurements Division CEA-13-125UN-120 strain gauge characterised by the following parameters:

Resistance	$(120.0 \pm 0.4)\,\Omega$
Gauge factor	2.11 ± 0.01

The gauge has been glued to the nozzle with cyanoacrylate as in Figure 1.17. The nozzle was screwed on a cylindrical test chamber connected to a compressor that constituted the gas source. The strain gauge output was detected via a Wheatstone bridge (Figure 1.17). The Wheatstone bridge transducer was realised using an instrumentation amplifier (INA111, Texas Instruments). The amplifier gain was set to $G_{ina} = 1000$. The strain gauge length is 3.18 mm and considering the maximum estimated strain of the nozzle body $\Delta L \approx 1\,\mu\text{m}$ (at $P = 20\,\text{bar}$) we get:

$$\frac{\Delta L}{L} \approx 3 \times 10^{-4}.$$

The variation in terms of gauge element resistance is:

$$\frac{\Delta R}{R} = G\frac{\Delta L}{L} \approx 6 \times 10^{-4}.$$

The resistor values in our Wheatstone bridge (as shown in Figure 1.17) are $R_1 = R_3 = 115\,\Omega$ and $R_2 = 120\,\Omega$. R_{sg} is the strain gauge resistance. A variation of the gauge resistance of $\frac{\Delta R}{R} \approx 6 \times 10^{-4}$ change the output of the bridge of $\Delta V_{bridge} \approx 1.4 \times 10^{-3}\,\text{V}$. The expected maximum output signal is given by the bridge voltage variation times the instrumentation amplifier gain $\Delta V_{out} = \Delta V_{bridge} G_{ina} \approx 1.4\,\text{V}$.

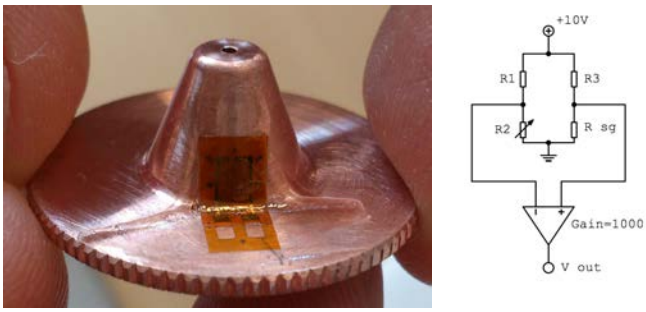

Figure 1.17: Left: gauge glued on the nozzle. Right: schematic representation of the Wheatstone bridge read-out circuit.

1.4.3 Results

Despite the attended read-out value of the strain gauge deformation was $\approx 400\,\mathrm{mV}$ for a 6 bar pressure applied to the nozzle, during our tests we didn't register any variation on the output signal. The noise level of the amplifier output was in the order of $10\,\mathrm{mV_{rms}}$, so the deformation of the nozzle caused by a 6 bar pressure was expected to be detectable. The failure of this type of measurement could depend on either the fact that the strain gauge was not positioned correctly on the nozzle body or the fact that the numerical simulation overestimated the nozzle deformation. For the future developments of this technique it is important to check the mechanical constrain used during the numerical simulation, and, on the other hand, for the strain gauge positioning, it is important to find the right place where the deformation reaches its maximum value, because the intensity of the deformation is not constant on the nozzle surface.

1.5 Conclusions

During the IPSP2014 week we reviewed different experimental techniques aimed at characterising the pressure and velocity field of the assistant gas flowing inside and outside a cutting machine head. We successfully realised a schlieren apparatus and performed qualitative pressure measurements of the gas ejected from the nozzle in various conditions. A novel sensor based on optical fibers was proposed and successfully tested during the IPSP2014 week.

Bibliography

[1] C. G. Lomass. *Fundamentals of Hot-Wire Anemometry.* Cambridge Univ. Press., 1986.

[2] Dantec Dynamics. Probes for hot-wire anemometry. `www.dantecdynamics.com`, 2012.

[3] Laser doppler anemometry. http://goo.gl/Q1EVgg.

[4] J. H. Whitelaw F. Durst, A. Melling. *Principles and practice of Laser-Doppler Anemometry*. Academic Press, 1981.

[5] G. S. Settles. *Schlieren and Shadowgraph Techniques, Visualizing Phenomena in Transparent Media*. Springer, 2001.

[6] Y. Haga K. Totsu and M. Esashi. Ultra-miniature fiber-optic pressure sensor using white light interferometry. *Journal of Micromechanics and Microengineering*, 15.1:71, 2005.

[7] Wikipedia.org. Fabryprot interferometer. http://goo.gl/Wi8OoO.

[8] S. Cova. Estensimetri o strain gauges. http://goo.gl/QgzMAS.

[9] Wikipedia.org. Drag (physics). http://goo.gl/QFsTVE.

CHAPTER

TWO

IDENTIFICATION OF COLORED-MASTERBATCH PROCESS-PARAMETER WITH GREATER INFLUENCE ON PIGMENT DISPERSION AND COLOR PERCEPTION

F. Benetti, M. Buccella, A. Caciagli, N. Cozza, F. Deirmina, D.M.S. Sultan, G. Giusti, E. Schneider, S. Tondini

Abstract

Aquafil S.p.A. has been one of the leading players in the production of Nylon 6. Over 60 % of its total production is composed by the so called solution dyed industrial yarns. The fibers are colored through a mass pigmentation process by the addition of Color Masterbatch during the melt spinning. From the industrial point of view, the most important problem for the Color Masterbatch production is to maximize the tinting strength of the color pigment. This have to be achieved by optimizing the fillers dispersion into the polymer bulk without using the dispersing additives, that can show detrimental effect during melt spinning. The dispersion degree of the pigments is the key point of the masterbatch production process and it depends on the physical properties of pigment particles, on the process parameters involved during extrusion and on the pigment concentration in color masterbatch. During IPSP2014, the Aquafil team of students and researchers worked on the realization of two models, one empirical and one theoretical, that could reproduce and predict the tinting strength of the Color Masterbatches, starting from the production process parameters. At the end of the week, the two developed models were able to qualitatively reproduce the experimental results measured on a set of Monoconcentrated Color Masterbatches, which were realized for this purpose by Aquafil during the event. Moreover, both models suggest that a critical production parameter for the realization of masterbatches with optimized tinting strength is the temperature profile of the extruder barrels.

2.1 Introduction

Since 1969, Aquafil[1] has been one of the leading players, both in Italy and globally, in the production of Nylon 6: a landmark in terms of quality and product innovation as, additionally, the Group is a leader in the research of new production models for sustainable development. This commitment to research and development leads to the regular renewal of processes and products thanks to continuous investments of capital and knowledge.

The Group has a presence in seven countries on three continents with 14 plants employing more than 2,200 people in Italy, Slovenia, Croatia, Germany, the United States, Thailand and China.

It operates through two product business units:

- BCF: production of filaments for textile floorings
- NTF: synthetic fibers used in the apparel and sports industries

Always committed to taking real measures to protect the environment, Aquafil established the Energy & Recycle business unit in 2008. This division is dedicated to the promotion of the research activities and sustainable projects, for all the Group's activities. The mission of Aquafil is to be the leader in the production of synthetic fibers, particularly Polyamide 6. To concentrate resources, ideas and investments on growth and excellence with the focus of environmental, social and corporate sustainability.

2.1.1 Colored masterbatch production

Over 60 % of the total production in Aquafil S.p.A. is composed by the so called solution dyed industrial yarns. The fibers are colored through a mass pigmentation process by the addition of color masterbatch during the melt spinning. The production of Color Masterbatch (CM) can be divided in two steps:

1. Production of Monoconcentrated Masterbatches (MM): they are obtained introducing one type of color pigment into the polymer matrix by an extrusion process
2. Production of Color Masterbatches (CM): they are obtained by mixing different kind of Monoconcentrated Masterbatches through an extrusion process, in order to reach the right color requested by the costumer.

Monoconcentrated Masterbatches are composite materials, also called concentrates, obtained by a melt compounding process, with a high amount of pigment (5-50 %wt.), higher than in the final products. Polymer matrix and one type of color pigment are mixed by an extrusion process, in order to obtain a fine dispersion of particles into the polymer. Monoconcentrated masterbatches are marketed in chips form and they are used in later production step for coloring plastic materials. During extrusion two mixing phenomena occur: (i) dispersing mixing that

[1] Aquafil S.p.A. website: `http://www.aquafil.com/`

breaks down the agglomerates in aggregates and primary particles and (ii) distributive mixing that produces an homogeneous distribution of pigment inside the polymeric matrix.

Color pigments used in plastic industry can be divided into two groups: inorganic and organic pigments. Their primary particles can have different shapes: cubes, platelets, needles or different irregular shapes. The primary particles of the most used pigments are composed by tiny molecular crystals, and show dimensions ranging from 20 to 500 nm. For this reason they are called nano colorants. Generally speaking, color pigments for plastic have to satisfy some requirements: (i) total insolubility in the polymer in which they are incorporated, (ii) easy dispersion within the matrix, (iii) chemical stability under severe thermo-mechanical processing conditions, (iv) compatibility with the other additives used, (v) nontoxicity and (vi) environmental friendliness. The most critical pigments to disperse in a polymer matrix are the organic ones and in particular the Copper Phthalocyanine Pigments (Blue and Green) and the Dioxazine Pigments (Violet). This is due to the high interface energy formed between pigment and polyamide that the system tends to reduce through flocculation.

2.1.2 Production process

In Aquafil S.p.A. the Monoconcentrated Masterbatches are produced through a co-rotating twin screw extruder because of its modular configurations that makes it flexible for adapting to changing tasks and material properties. The extrusion process is characterized by the properties of the extruder (i.e. power, L/D, the screw geometry) and the variable parameters (i.e. screw speed, throughput rate, ampere absorption, pressure at spinneret, temperature profile) and the quality of the product are strongly depended on these process features.

The schematic layout of the monoconcentrated masterbatch process is represented in Figure 2.1. The polymer powders, stored in the controlled atmosphere silos, and the color pigments have been weighted and moved into a container mixer. By a so called turbo-mixer machine the powders compound is premixed to make the materials feeding as much uniform as possible. Through a volumetric dosing unit the compound is fed into extruder in which the real mixing occur. At the end of extrusion, the polymer mixed with the pigments is forced to pass through a spinneret and the filaments produced are cooled down by water and by air before going into pelletizer, that produces the chips of monoconcentrated color masterbatch (3 mm).

2.1.3 Industrial problem

From the industrial point of view, the most important problem for the Color Masterbatch production is to maximize the tinting strength of the color pigment. This have to be achieved by optimizing the fillers dispersion into the polymer bulk without using the dispersing additives, that can show detrimental effect during melt spinning [1].

The dispersion degree of the pigments is the key point of the masterbatch production process and it depends on the physical properties of pigment particles

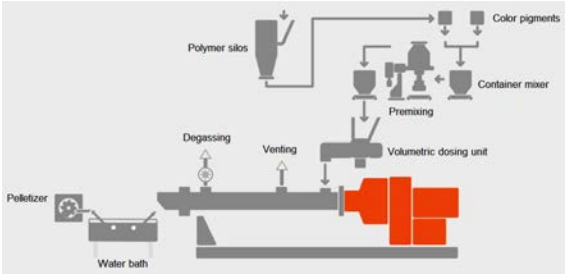

Figure 2.1: Schematic representation of monoconcentrated masterbatch production process.

(i.e. size, shape, surface properties, crystalline structure, chemical composition of the primary crystals), on the process parameters involved during extrusion (i.e. screw speed, throughput rate, temperature profile) and on the pigment concentration in color masterbatch.

This problem shows an important industrial relevance because an improvement of the pigment dispersion allows to reduce the clogging phenomenon and the filament breakage during melt spinning, thanks to the reduction in agglomerates' dimension. This results in an improvement of the productivity and the stability of the production process. Moreover, the reduction of the pigment agglomerate dimension leads to an increment of the light absorption. The consequent enhancement of the pigment color strength allows to reduce the concentration of the monoconcentrated masterbatch and so to reduce the cost of production.

2.2 Experimental investigation

2.2.1 Samples production and characterization

Samples production

The samples were produced by using a lab scale extruder, in order to be able to control and change all parameters during the production. In Figure 2.2 the picture of the adopted *LabTech* extruder is reported.

The monoconcentrated masterbatch were obtained using different parameters in order to find the right combination that allows an increase in the color strength of the final product. The algorithm used to find the appropriate set of parameters for the trials is explained in detail in section 2.2.3. As a quick reference, the interested reader can find this set in Table 2.1.

Color strength evaluation

The color strength identifies the property of a pigment to impart color to a substrate under specific processing conditions [2, 3]. The reflectance curves of samples were determined through a *Hunterlab*® *Colorquest XE* Spectrophotometer. The measured reflectance of an optically infinite thick layer $R_\infty(\lambda)$ is related to the ra-

Figure 2.2: Photograph of the extruder used in the sample production.

tio of the absorption coefficient $K(\lambda)$ and the scattering coefficient $S(\lambda)$ for diffuse light according to the two-flux radiation theory of Kubelka-Munk (KM) [4]:

$$\frac{K(\lambda)}{S(\lambda)} = \frac{(1 - R_\infty(\lambda))^2}{2 \cdot R_\infty(\lambda)}$$

The relative color strength (RCS) was determined comparing the K/S ratio of the sample and that of a standard reference [5], as given by

$$RCS = 100 \cdot \frac{(K/S)_{\text{sample}}}{(K/S)_{\text{reference}}}$$

RCS determination is an indirect method to have an idea of the pigment dispersion inside the matrix: the higher RCS values, the better dispersion is achieved [6, 7].

End groups analysis

End groups analysis was performed on extruded pellets, in order to investigate the effect of the different processing conditions on the chemical properties of the monoconcentrated masterbatches. These tests were performed by using a *Mettler DL50* automatic titrator coupled with an electronic voltmeter [8]. About 0.8 g of samples were solubilized in 20 ml of *2,2,2 trifluoroethanol* (TFE) at 55 °C. -NH_2 groups titration was performed at 25 °C through a HCl 0.02 N solution, while -COOH titration was carried out with a NaOH 0.02 N solution. The adopted testing methods have been previously optimized, such that the absolute error associated to each measurement is in the order of 1 mmol kg^{-1} [7].

2.2.2 Introduction to the Design Of Experiment

The DOE is a method to select samples in the design parameters space, in order to obtain maximum information using minimal resources. There are several ways of

choosing an optimal sample arrangement, from which different informations can be retreived [9]. The statistical approach to experimental design is the preferred one when meaningful conclusions have to be derived from the collected data even if those are subject to errors and/or randomness of the input values.

An effective approach to lead experiments with multiple factors consists in the realization of a factorial plane, in which the factors vary jointly instead of one at a time (see Figure 2.3). A very important feature of factorial experiments is the high efficiency in using the experimental data [10].

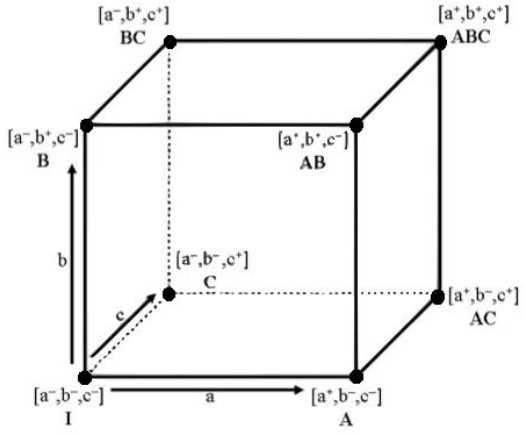

Figure 2.3: Graphical representation of a full factorial design with 3 factors a, b, c, each one on 2 levels: $-$ and $+$.

In general, when all the factors are investigated with the same number of levels, this is called a family of factorial planes with L levels and k factors (L^k). A factorial plane is said to be complete (full factorial) when using all possible combinations of factor levels. In this case the number of tests required for a complete characterization of the system is L^k. A full factorial design also allows for the calculation of the interaction between the factors. As an example, among the trials of Figure 2.3, we find 4 configurations where a and b share the same level ($-$ or $+$), and 4 configurations where the two factors lie in opposite levels. From these it is possible to calculate the effect of the interactions of a with b, of a with c, and so on.

A common approach in the DOE is the approximation of the system with a linear model. As an example, the equation representing the system of Figure 2.3 would be

$$Y = x_0 + x_a a + x_b b + x_c c + x_{ab} a \cdot b + x_{ac} a \cdot c + x_{bc} b \cdot c + x_{abc} a \cdot b \cdot c$$

By comparing the coefficients of the model, it is possible to determine which factors contribute more to the system response. A possible way to check the quality of the result is to look whether there could be a physical explanation consistent with the process under study.

When the number of involved factors increases, the number of points grows exponentially and the number of trials may not be sustainable. In such cases, it can be helpful to use a fractional factorial design [11]. To this regard, Taguchi [12] proposed an improved DOE that simplifies and standardizes the factorial and fractional factorial designs so that the conducted experiments can produce more consistent results. The major contribution of the work has been in developing and using a special set of orthogonal arrays for designing experiments. Orthogonal arrays are a set of tables of numbers, each of which can be used to lay out experiments for a number of experimental situations. Through the orthogonal arrays, it is possible to carry out fewer fractional factorial experiments than full factorial experiments. Also, the relative influence of factors and interactions on the variation of results can be identified. Through fractional factorial experiments, optimal conditions can be determined by analyzing the relative color strength (RCS) as a performance measure, employing different Statistically Process Control tools (SPC) [13]. The details of this investigation has presented in the following subsections.

2.2.3 Sample selection strategy

Choosing the right test cases in the beginning is always crucial for the successful DOE. The yields of the experiment, i.e. the RCS of the polymeric fiber, can be optimized by varying T (Temperature), n (Screw rate), Q (Throughput) and P (Electrical power) of the extruder System. Considering the industrial know-how of the production system of Aquafil, T (temperature), n (screw rate), and Q (throughput) were considered as the controllable factor to the DOE (see Figure 2.4).

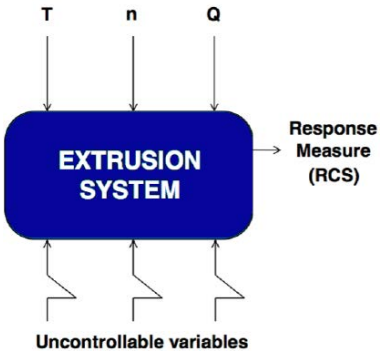

Figure 2.4: Schematic representation of the extrusion system where T (Temperature), n (Screw rate) are the controllable factors and Outcome of the experiment is RCS. Uncontrollable factors to the experimentation are ambient temperature, humidity etc. that could act as the noise of the system.

The choice of the sets of processing parameters to be tested, however, have to deal with the following constraints:

- not feasibility of some parameters configuration in terms of outcoming product;
- inclusion of the standard working condition into the trials to be performed;
- no more than 8 measurements.

This led us to propose an hybrid DOE based on a 3-factor 2-level fractional factorial design, where vertical array test sets have taken into account during the appliance of DOE. As in Figure 2.5 (Left), vertical array elements (black circled) have chosen as optimal candidate for fractional factorial design.

By looking at the scheme, we do see that, among all the $[T, n, Q]$ possible configurations, the ones with levels $[-1, -1, -1]$, $[+1, -1, +1]$, $[+1, +1, -1]$ and $[-1, +1, +1]$ are missing because they cannot be physically realized. Moreover, the standard working condition, represented by the point $[-1, 0, -1]$, has been included into the necessary tests.

The choice of vertical test sets for fractional choice are eminent because they ensure the elimination of a non-affecting variable (that can be observed by Pareto Plot, produced in R) still essentially providing the data for a full factorial design on the other two variable. For example, if it could be confounded from the pareto plot that the throughput Q has rare impact on the outcome RCS, then Q could be eliminated leaving the opportunity to analize a full factorial DOE with T (Temperature) and n (Screw speed).

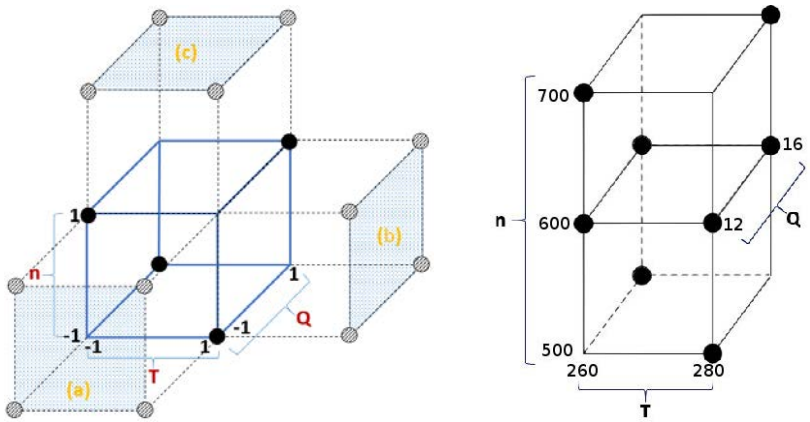

Figure 2.5: (Left) Cube representation of fractional factorial design, where black circles represents the chosen vertical array test sets. (a), (b) & (c) planes represents the possible full factorial representation of n & T, n & Q and T & Q controllable variables. (Right) Cube representation of fractional factorial design of T, n, and Q.

Following the instrumental safety guidelines and recommendation of production-line experts of Aquafil, the values of controllable factors reported in Table 2.1 were considered. To represent the composition of T, n, Q with 2, 3, and 2 levels, respectively, the cube facets of Figure 2.5 (Left) turns into the ones of Figure 2.5 (Right).

To limit the effects of uncontrollable variables within the DOE, the set of experiments have been performed using random appliance to standard (std.) order. The retrieved yields (RCS) for each run (performed in Aquafil) can be summarized in Table 2.1.

Table 2.1: Selected parameters for sample production and outputs of the experimental and theoretical analysis.

Sample number	1	2	3	4	5	6	7	8
Temperature (°C)	260	260	260	260	280	280	280	280
Screw Rate (rpm)	600	600	500	700	600	600	700	500
Throughput ($\mathrm{kg\,h^{-1}}$)	12	16	16	12	12	16	16	12
RCS enhancement (%)	0	3	4	1	12	7	6	2
Mean diameter $\bar{d}$ (nm)	87	84	93	81	58	59	53	65
N° end groups ($\mathrm{mmol\,kg^{-1}}$)	106	104	104	106	103	106	103	104

2.2.4 Analysis of data

The experimental data have been processed with Statistical Process Control (SPC), while to obtain the causal analysis on yields, Pareto Plot is calculated using R[2]. According to a common prescription in data science, interactions of order higher than 2 in linear regression model dont have a significant effect on yields. As appears from the Pareto Plot of Figure 2.6 (Left), it is quite probable that positive changes in T and negative changes in $n \cdot Q$ interaction have the greater influence on yields.

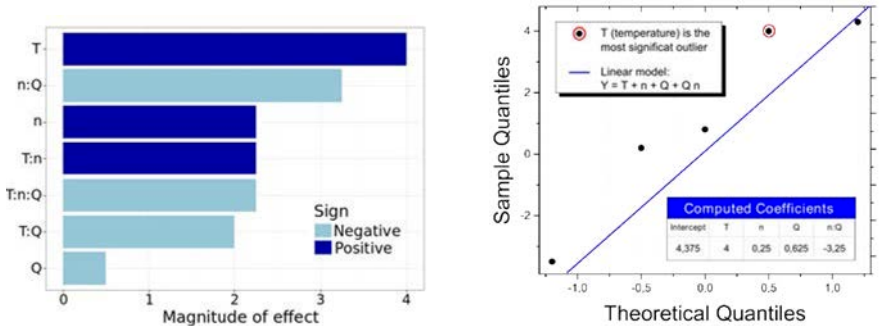

Figure 2.6: (Left) Pareto Plot of the linear model of DOE. Inset showing the color code (sign) of Estimates of the linear model. (Right) Quantile-Quantile normal distribution plot.

At this point, the linear regression model was readjusted and then verified with Quantile-Quantile (Q-Q) Plot, as represented in Figure 2.6 (Right). A Q-Q plot is a plot of the quantiles of the first data set against the quantiles of the

[2]R Foundation for Statistical Computing, `http://www.R-project.org`

second data set. This graphical investigation ensures if two data sets come from populations with a common distribution. Also in this approach, it can be seen that T is the most significant outlier. Thereby, the change in temperature will make the most significant change in the RCS yield.

The first test performed to validate the linear model is the ANalysis Of VAriance (ANOVA) [14]. ANOVA is the statistical tool that is used to check regression model significance. Normally, a model is considered suitable if the Sum Square (SS) of the unmodelable variation, SS_{residual}, is low compared to the modeled values, $SS_{\text{regression}}$. The variance is obtained by dividing the SSs by the corresponding degrees of freedom. The sizes of these two variances are evaluated by the F-test. Commonly, $p = 0.05$ is set as the critical limit, which means that if $p < 0.05$, the variance explained by the retained model is significantly larger than the unexplained variance.

Table 2.2: Regression for Temperature vs RCS

Fitted line: $Y = 262.1 + 1.795 \cdot x$			
	Selected Model	Alternative Models	
	Linear	Quadratic	Cubic
R-squared (adjusted)	33 %	23 %	9.7 %
p-value, model	0.08*	0.22	0.40
p-value, linear term	0.08*	0.33	0.95
p-value, quadratic term	–	0.65	0.69
p-value, cubic term	–	–	0.65
Residual standard deviation	8.7	9.4	10

*Statistically significant $p < 0.1$

The second statistical test performed is the analysis of residuals, where the difference between linear model and the observed output is checked. Goodness of linear model is approved if the residuals are distributed randomly for all variable ranges and modeled responses (outputs). To find the interaction effect of n and Q on the yield, a simple numerical investigation is done in "R" environment.

According to this linear model, $\text{F}_{\text{critical}}=\text{F}(2, 21)$ is 3.5 at $\alpha = 0.05$, where 2 and 21 are the degree of freedom between groups (f_B) and degree of freedom within group (f_W), respectively. From the results of anova, F-test value of T is $3.7 > 3.5$, which means that the result is significant at the 5 % significance level. On the contrary, F-test value of the interaction $n \cdot Q$ is 1.7, which is lower than $\text{F}_{\text{critical}}$ and, thereby, proves its statically insignificance to the effect on yields.

2.2.5 Degradability estimation

End groups analyses were performed in terms of aminic and carboxylic functionalities on all samples produced, in order to evaluate the degradation effect of each production set-up. In Table 2.1 the sum of end groups for all production are reported. It is possible to notice that no significant variation were detected, even

by using higher temperature profile during the production.

2.3 Theoretical model

2.3.1 Problem breakdown

In parallel to the experimental investigation discussed so far, we decided to address the problem proposed by Aquafil also from a more theoretical point of view. The results provided by the DOE method, in fact, are very useful, but their validity is limited to the range of the tested parameters. In this view, the development of a theoretical model able to reproduce experimental result could provide insight into the extrusion process.

A general model of the extrusion process is very difficult to provide, due to the number of mechanisms involved and the complexity of the underlying physical phenomena [15, 16]. For this reason, it is very important to reduce the problem complexity by highlighting from the beginning the more relevant phenomena. One of the most important microscopic parameters in the masterbatch is the final size of the agglomerates. This characteristic is empirically found to be directly related to the color quality of the texture. Namely, a small molecular aggregate at the end of the extrusion process results in a higher RCS value of the masterbatch.

Thus, the purpose of our theoretical model is to provide a link between the external macroscopic parameters directly tunable in the extrusion procedure (temperature T, throughput Q, and screew speed ω) and the final agglomerate size d. The goal is to identify an optimal configuration of the production parameters.

As said above, though, a complete general description of the overall process is unfeasible. We therefore chose to divide the underlying physics into two separate domains: the *macroscopic* and the *microscopic*. In both these domains, a set of quantities represent the input parameters and another set represent the output ones. For the macroscopic domain, the input set consists of the extruder parameters, while the output set is represented by the melt physical attributes. At the microscopic level, on the contrary, the input set is now represented by the melt attributes, while the final output is the pigment cluster size.

2.3.2 Macroscopic description

In this section, we model the extruder in terms of different geometries and parameters conditions (i.e. temperature). To simplify the treatment, we assume a constant speed of the melt during the extrusion process, matching time of residence and position in the extruder for any particle in the melt [17].

The model specifications are proper of the extrusor machine used by Aquafil S.p.A, which consists of 10 sectors. The total time spent in the machine by a bunch of pigment is approximately 15 s, resulting from empirical considerations. Thus, we model the pieces of the screw by dividing the process time in 10 sections, each lasting 1.5 s, following the assumption of a constant speed of the melt as stated above. In each sector we consider a different screw geometry, which result in a

Table 2.3: Parameters to compute viscosity

η_0 $[s^{-1}]$	η_{1000} $[s^{-1}]$	n_{visc}	C_{visc} [s]	E_{act} $[J\,mol^{-1}]$	T_0 [K]
323	195	0.453	0.0019	-100	533

different shear rate, and a different temperature. In Figure 2.7 the set temperature profile and shear rate profile along the extruder are shown.

As it will be shown later, in order to simulate the time evolution during the extrusion process of the average cluster pigment d,the evaluation of the fluid shear stress and the critical shear stress is very sensible.

- **fluid shear stress**: this quantity is the product between the local viscosity of the medium on the cluster, η, and the shear rate, a quantity related to the rotational energy transmitted to the melt:

$$\tau_{fluid} = \dot{\gamma}\eta \ .$$

The average shear rate depends on the geometry of the extruder, the screw speed and the throughput [18],

$$\dot{\gamma}(\omega, Q) = \mathrm{k}\omega^{\alpha(Q)} \ ,$$

where α is a constant to account for material conveying in the extruder, depending principally by the throughput

$$\alpha(Q) = 1.5 - (1 - Q/Q_{max}) * 0.2$$

and k is a parameter depending on the given type of screw geometry. We identify three different region, with different value of $k_i = 8,\ 8.5$ and $10\,\mathrm{rpm}^{\alpha}\mathrm{s}^{-1}$, where the maximum value identifies the kneading blocks in the screw. The value Q_{max} is fixed at $16\,\mathrm{kg\,h}^{-1}$.

We express the viscosity as follows,

$$\eta(T, \omega, Q) = \left(\eta_\infty + \frac{\eta_0 - \eta_\infty}{(1 + C_{visc}\dot{\gamma})^{n_{visc}}}\right) e^{E_{act}/R(1/T - 1/T_0))}$$

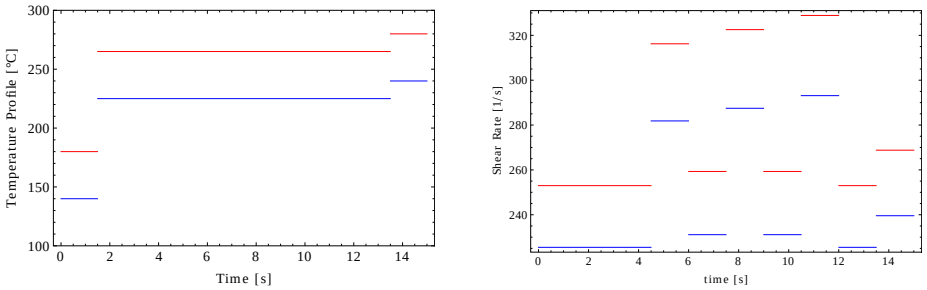

Figure 2.7: (Left) Two examples of set temperature profile along the extruder. (Right) Shear rate profiles corresponding to the curves in the left plot. Note the high shear rates given by the kneading blocks.

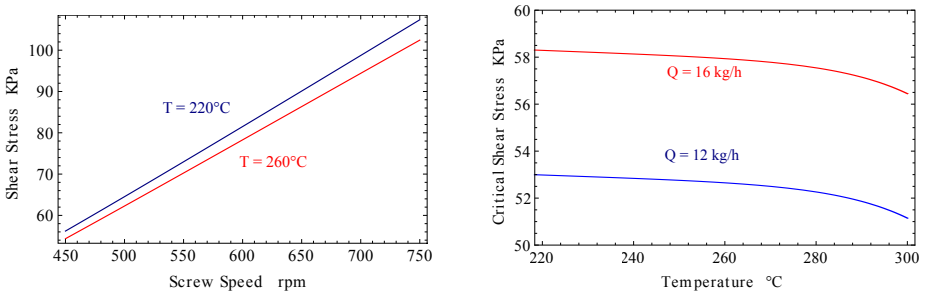

Figure 2.8: (Left) Fluid shear stress versus screw speed for two different temperatures T. (Right) Critical shear stress versus temperature for two different throughput values Q.

where η_0 is the viscosity in absence of screw rotation, and η_∞ at ideally infinity shear rate. The exponential factor is crucial to take in account thermal effects, which follow an Arrhenius law. The parameter used are reported in Table 2.3.

- **critical shear stress**: to accurately describe this quantity, a deep insight into the properties of the extruder and, especially, the pigment would be needed. However, we find reasonable that at the beginning of the extrusion process an ideal equilibrium state between these two stresses is present. Thus, we fit the free parameter to have a ratio $\pi_B \approx 1$ at $t = 0$.

In Figure 2.8 (Left) we show the local fluid shear stress dependence versus the screw speed input parameter (ω) at two different value of temperature (T), while in Figure 2.8 (Right) we show the critical shear stress dependence on the temperature (T) and throughput (Q).

2.3.3 Microscopic description

The cluster size of the pigment can be modeled as the result of the competition between three different physical processes: agglomeration, erosion and fragmentation [17]. The smallest size is reached when the agglomeration rate is overcome by the combination of the erosion and fragmentation mechanisms.
The formula that describes the change in the agglomerate diameter d over time can be expressed, in its simplest form, as a linear superimposition of the three mechanisms:

$$\frac{\partial d}{\partial t} = \frac{\partial d}{\partial t}_{\text{Agglom.}} - \frac{\partial d}{\partial t}_{\text{Rupture}} - \frac{\partial d}{\partial t}_{\text{Erosion}} ,$$

where $d(t)$ is the average cluster size at residence time t. According to the literature on the topic [17, 19], the three processes can be described separately by

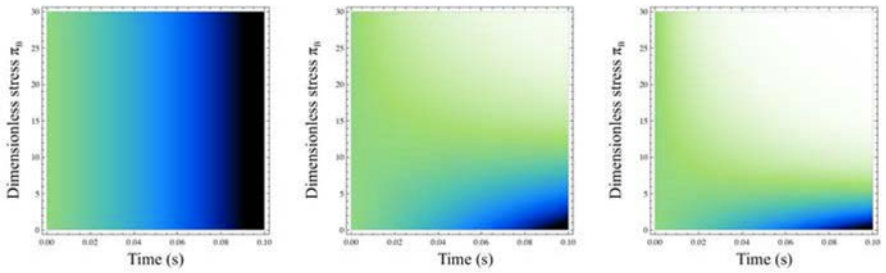

Figure 2.9: Agglomerate size time dependence depending on the dimensionless shear stress ratio $\pi_{\mathrm{B}} = \tau_{fluid}/\tau_{sch}$. Left plot include only agglomeration contributions, central plot agglomeration and erosion, right plot all the competing phenomenas. Dark region represent bigger cluster size and light region smaller cluster size.

linear differential equations:

$$\frac{\partial d}{\partial t}_{\text{Agglom.}} = \frac{1}{8}\left(1+\sqrt[3]{2}\right) c_{so}\dot{\gamma} d \tag{2.1}$$

$$\frac{\partial d}{\partial t}_{\text{Rupture}} = \frac{5}{256}\frac{\tau_{fluid}\ \dot{\gamma}}{\pi\left(1-\epsilon\right)\tau_{sch}} d \tag{2.2}$$

$$\frac{\partial d}{\partial t}_{\text{Erosion}} = \frac{5}{128}\frac{\tau_{fluid}\ \dot{\gamma}}{\pi\tau_{sch}} d \tag{2.3}$$

where c_{so} is the pigment concentration, $\dot{\gamma}$ is the viscosity, ϵ is the porosity of the pigment cluster, τ_{fluid} and τ_{sch} are respectively the shear stress of the polymer melt and the critical shear stress of the cluster. It should be noted that Eq: 2.2 and Eq: 2.3 strongly depend on the ratio between the two shear stresses, $\pi_{\mathrm{B}} = \tau_{fluid}/\tau_{sch}$.

Figure 2.9 shows the time evolution of the cluster size $d(t)$ for different values of π_{B}. The plot on the left only considers the agglomeration mechanism. The plot at the center shows the interplay between agglomeration and erosion. Finally, the plot results in including all the three contributions. It should be stressed that, in order to achieve the optimal result (i.e. to reduce the size of the agglomerates to a minimum value), the shear stresses during the process have to overcome a critical value.

2.3.4 Theoretical outcomes

Finally we can combine the previous equations to simulate the evolution of the average cluster size d for different values of inputs (T, Q, and ω). In Figure 2.10 we report two different curves: one at high and one at low temperature. We point out the presence of three really steep behavior, which correspond to the kneading blocks in the screw.

The implementation of this really simplified theoretical model seems to confirm the outcomes of the experimental analysis. We have shown that the model predicts

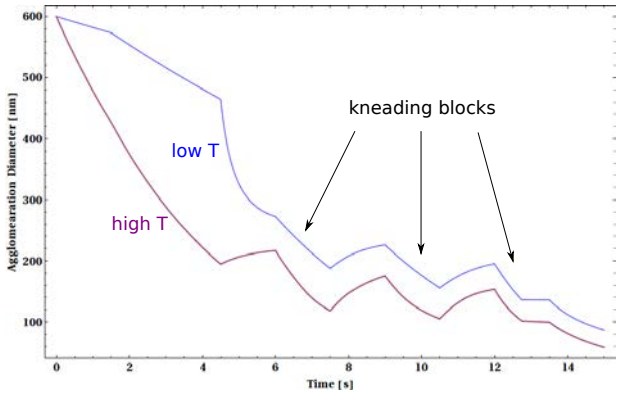

Figure 2.10: Size of the agglomerates as a function of the residence time in the extruder for two values of temperature.

a lower final pigment cluster d for a higher set temperature T. A more detailed comparison between experimental and theoretical data is shown in Table 2.1, in which we observe a qualitative inverse correlation between the final cluster size d and the RCS value.

Lastly, we warn here that our model does not take into account the filament mechanical quality, which is well beyond the scopes of this analysis. For this reason, the processing parameters which are optimal to obtain higher RCS values are not necessarily optimal also for what concerns the colored fiber mechanical quality.

2.4 Conclusion

One of the most important issues related to industrial production of color masterbatch concerns the optimization of the extrusion process in order to maximize the tinting strength of the color pigments [1].

The aim of the work presented in this article regards the development of a model, supported by experimental data, able to predict how the coloration quality of masterbatch is affected by the operative parameters of the extrusion. The operative parameters include the screw speed, the throughput and the mean temperature along the extruder. An accurate setting of these parameters could lead to important advantages in terms of working time and materials consumption.

The model, proposed in this work, is based on the theoretical description of the physical mechanisms occurring during the extrusion process and on some data regarding the physicochemical properties of the materials involved. The model provides previsions about the size of the pigment clusters at the end of the extrusion process approaching the problem on two complementary scale levels: the macroscopic level and the microscopic level. At the macroscopic level, the local attributes of the extruder (shear stresses, viscosity, etc.) are calculated starting from the values of the extrusion parameters using mathematical approaches

provided by previous works. The so-calculated attributes and the physicochemical properties of the pigment materials are the inputs for the model concerning the microscopic level. Three phenomena are considered to occur to the pigment clusters at this level: the erosion, the fragmentation and the agglomeration of the clusters. The solution of the whole equation system provides the average diameter of the pigment clusters. The information about the size of the pigment clusters can be directly related to the quality of the tinting strength of the pigment embedded into the masterbatch. In particular, lower size of the pigment clusters lead to higher coloration quality, as demonstrated in previous works.

The goodness of the theoretical model was tested by experimental measurements consisting in the RCS evaluation of the samples produced setting the extruder parameters in a realistic range of values. The RCS values are directly proportional to the coloration quality of the samples. The RCS data were acquired using a spectrophotometer. Due to the cost and the time consumption required the sample preparation, the choice of the parameter set for each sample was carefully weighted. In particular, advanced techniques of Design of Experiment were employed in order to analyze all the space of parameters.

The results reveal a high degree of correlation between the RCS values of the analyzed samples and the diameters of the pigment clusters predicted by the model. This evidence provides a confirmation of the goodness of the theoretical model. It is remarkable that the mean temperature along the extruder is recognized as the most important parameter in the determination of the masterbatch quality for the operative range considered in this study. In particular, the higher value of mean temperature was associated to the better results in terms of coloration quality. The suitability of the temperature range considered in this work was proved by titration analysis of the terminal groups of the polymer molecules. The data allow excluding higher degradation of the polymer in the sample produced at higher mean temperature.

In conclusion, a reliable tool supported by experimental validation and suitable for quality predictions was developed. The information provided by this tool could allow the identification of the best set of parameter values in order to reach an effective optimization of the industrial production.

Improvements of this model can be reached considering other aspects of the production process: the possibility to produce masterbatch by multiple extrusion processes and/or the insertion, into the model calculations, of the temperature profile along the extruded rather than the mean value only.

Other experimental techniques may be used to evaluate the accuracy of the model. For example, microanalysis techniques, like EDAX and XPS, can provide information about the size of pigment cluster for a direct comparison with the theoretical model outcomes. Preliminary considerations about the employment of XPS analysis in this kind of studies are reported in section 2.5.

Considering the industrial relevance of masterbatch production, the model proposed in this work can provide relevant economic benefits, although further studies are required in order to provide a robust statistics supporting model reliability before real implementation.

2.5 Addendum: XPS analysis

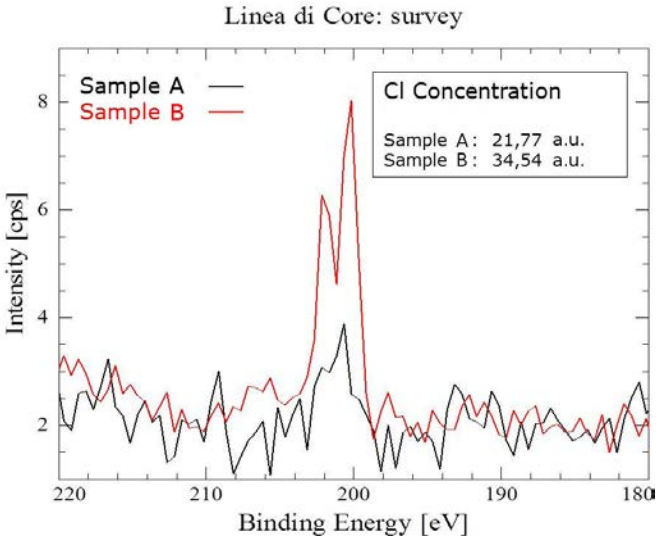

Figure 2.11: XPS analysis of single-extruded sample (Sample A) and double-extruded sample (Sample B). In the box, the superficial concentrations of chlorine in each sample are reported.

In this part of the work, the suitability of X-ray photoelectron spectroscopy (XPS) as analysis technique to study the pigment dispersion inside the polymer matrix of color masterbatch has been evaluated. Process based on multiple extrusions was employed to produce samples with remarkable differences in terms of pigment cluster size. In fact, as shown in a previous study [7], multiple-extruded masterbatches reveal higher color strength compared to samples processed once, suggesting a better pigment dispersion. Two samples have been produced by single and double extrusions, respectively, using the same quantity of polymer and pigment. As expected, the optical characterization of the samples highlights that the RCS value of the double-extruded sample exceeded the RCS value (+10 %) of the single-extruded sample confirming better pigment dispersion in the double-extruded one. XPS measurements have been performed in order to estimate the amount of chlorine in the samples. The quantification of chlorine is thought to provide information about the degree of pigment dispersion inside the masterbatch. In particular, smaller pigment clusters are expected to expose greater pigment area to the electron probe compared to larger clusters leading to higher signal related to the chemical species composing the pigment compound. Considering the masterbatch system, chlorine is univocally associated to pigment molecules thus the measurement of the chlorine amount provides a direct estimation of the pigment cluster size inside the masterbatch. Figure 2.11 shows a remarkable difference in the XPS intensity of the chlorine peaks between the samples. This observation suggests that double-extruded sample contains larger pigment area exposed to the measurement beam, which relates to a cluster size

lower than the single-extruded sample. Therefore, the result of this preliminary analysis supports the employment of XPS technique for the study of pigment cluster size inside masterbatch in order to provide important information about the outcomes of production process.

Acknowledgement

We acknowledge the technicians of Aquafil, who helped in the sample preparation and characterization (RCS and chemical analysis). We also acknowledge the MateC Laboratory, from the "CMM - Centro Materiali e Microsistemi" of FBK, for the kind support and the XPS measurements.

Bibliography

[1] M. Buccella, A. Dorigato, F. Crugnola, M. Caldara, and L. Fambri. Coloration properties and chemo-rheological characterization of a dioxazine pigment based monodispersed masterbatch. *Journal of Applied Polymer Science*, 2014.

[2] H. Zollinger. *Color Chemistry: Syntheses, Properties, and Applications of Organic Dyes and Pigments*. Wiley & Sons Inc., 2003.

[3] G. A. Klein. *Industrial Color Physics*. Springer, 2010.

[4] I. Ariño, U. Kleist, and M. Rigdahl. Color of pigmented plastics - measurements and predictions. *Polymer Engineering & Science*, 44:141–152, 2004.

[5] W. Herbst and K. Hunger. *Industrial Organic Pigments: Production, Properties, Applications*. Wiley & Sons Inc., 2006.

[6] M. Lewin. *Handbook of Fiber Chemistry*. Taylor & Francis, 3rd edition, 2010.

[7] M. Buccella. *Color masterbatches for polyamide 6 fibers. Optimization of compounding and spinning processes. Physical-chemical characterization of industrial products*. PhD thesis, Dept. of Industrial Engineering, University of Trento, 2014.

[8] P. Ghosh. *Polymer Science and Technology: Plastics, Rubbers, Blends and Composites*. McGraw-Hill, 2001.

[9] A. C. Atkinson, A. N. Donev, and R. D. Tobias. *Optimum Experimental Designs, with SAS*. Oxford University Press, 2007.

[10] R. L. Mason, R. F. Gunst, and J. L. Hess. *Statistical design and analysis of experiments with applications to engineering and science*. Wiley, New York, 1989.

[11] M. J. Anderson and P. J. Whitcomb. *DOE Simplified: Practical Tools for Effective Experimentation*. Productivity Press, 2nd edition, 2007.

[12] R. K. Roy. *Design of experiments using the Taguchi Approach*. John Wiley & Sons, Inc., 2001.

[13] D. J. Wheeler. *Understanding Variation: The Key to Managing Chaos*. SPC Press, 2nd edition, 2000.

[14] N. R. Draper and H. Smith. *Applied Regression Analysis*. Wiley, New York, 2nd edition, 1981.

[15] H. Potente, M. Bastian, and J. Flecke. Design of a compounding extruder by means of the sigma simulation software. *Advances in Polymer Technology*, 18:147170, 1999.

[16] H. Potente and K. Kretschmer. Simulation and evaluation of compounding processes. *Macromolecular Materials and Engineering*, 287, 2002.

[17] J. Flecke, H. Potente, and K. Kretschmer. A physico-mathematical model for the dispersion process in a co-rotating intermeshing twin screw extruder. *Journal of Reinforced Plastics and Composites*, 21:507–515, 2002.

[18] M. Suparno, K. D. Dolan, P. K. W. NG, and J. F. Steffe. Avearage shear rate in a twin-screw extruder as a function of degree of fill, flow behavior index, screw speed and screw configuration. *Journal of Food Process Engineering*, 34:961982, 2011.

[19] H. Potente and K. Kretschmer. Simulation and evaluation of compounding processes. *Macromolecular Materials and Engineering*, 287:758–772, 2002.

CHAPTER

THREE

DEVELOPING A SENSORS TO MEASURE THE QUALITY OF ADBLUE®

S. Bacchi, M. Bianchi, Z. Bisadi, N. Cagol, M. Falciano, M. Guarisco, M. Valentini, M. Vardaro

Abstract

The Euro 6 European emission standard sets a limit of $0.080\,\mathrm{g\,km^{-1}}$ to NO_x emissions. A possible approach to bring the emissions of unburned nitrogen compounds below this limit consists in using a selective catalysis process obtained via injection of AdBlue® into the exhaust pipeline. Both the use of AdBlue® and its storage inside the vehicle present two main problems. The first problem is the possible refill of the storage tank with a substance different from AdBlue®, while the second is its degradation due to different evaporation rates of its components (i.e. water and urea). Our proposed solution is to integrate into the NO_x catalysis system a sensor capable of monitoring the status of the mixture. During IPSP2014 the Röchling group ran a feasibility study for the implementation of an AdBlue® sensor. The work was organized in two subsequent phases. During the first phase the group conducted a theoretical study to discover the possible physical properties exploitable in order to reveal anomalies in the solution. During the second step the group focused on the analysis of the electrical properties of the mixture, in particular impedance and resistance. During this phase we developed and characterized two sensor prototypes: an electrolytic sensor and a second sensor. In parallel we developed an embedded device able to measure both impedance and temperature in order to integrate the sensors in a automotive system.

3.1 Introduction

Most of the vehicles sold in EU member states are subject to an emission standard which fixates an upper level of polluting substances that they can emit. The emission standards are identified with the denomination Euro-n, where n is a

Table 3.1: European emission standards for diesel (D.) and gasoline (G.) vehicles. Limits are expressed in $g\,km^{-1}$ [1, 2].

Tier	Date	CO	THC	NO_x	HC^+NO_x	PM
D. Euro 1	07/1992	2.72	-	-	0.97	0.14 (0.18)
D. Euro 2	01/1996	1.0	-	-	0.7	0.08
D. Euro 3	01/2000	0.64	-	0.50	0.56	0.05
D. Euro 4	01/2005	0.50	-	0.25	0.30	0.025
D. Euro 5	09/2009	0.50	-	0.180	0.230	0.005
D. Euro 6	09/2014	0.50	-	0.080	0.170	0.005
G. Euro 1	07/1992	2.72	-	-	0.97	-
G. Euro 2	07/1996	2.2	-	-	0.5	-
G. Euro 3	07/2000	2.3	0.20	0.15	-	-
G. Euro 4	07/2005	1.0	0.10	0.08	-	-
G. Euro 5	09/2009	1.0	0.10	0.060	-	0.005
G. Euro 6	09/2014	1.0	0.10	0.060	-	0.005

progressive number, introduced by the European Union directives as progressive stages of emission upper levels. A higher number indicates a more recent standard, with more restrictive limits to exhaust emissions. The standards provide the maximum value of polluting gases that vehicles can emit, expressed in $g\,kW\,h^{-1}$ for large goods vehicles and in g/km for all the other vehicles classes. Vehicles which do not satisfy the standards imposed by EU can not be registered, while newer directives do not apply to already registered vehicles.

The pollutants regulated by these norms are: nitrogen oxides (NO_x), hydrocarbons (THC), non-methane hydrocarbons (NMHC), carbon monoxide (CO) and particulates (PM). These regulations are enforced for all vehicles types with the exception of sea ships and planes. Each group of vehicles is subject to a different standards. Table 3.1 reports the maximum values of emitted pollutants for diesel and gasoline vehicles.

The Euro 6 standard requires a severe reduction of NO_x emissions for diesel vehicles with respect to the Euro 5 counterpart. In particular it is required to reduce NO_x emissions from $0.180\,g\,km^{-1}$ to $0.080\,g\,km^{-1}$.

In order to meet this requirement, Röchling is aiming to achieve selective catalysis reduction (SCR) of the exhaust gas. The selective method used to catalyse NO_x into N_2 and H_2O consists in injecting a mixture of urea and water directly in the exhaust muffler, activating the following reaction:

$$NH_2 + 2\,CO + H_2O \rightleftharpoons 2\,NH_3 + CO_2 \rightleftharpoons NO_x + NH_3 + O \rightleftharpoons N_2 + H_2O$$

Figure 3.1 shows the basic scheme of the SCR system inside a vehicle.

One of the inconveniences of AdBlue® [3] is that water–urea mixtures have a relatively high freezing point. Figure 3.2 shows how freezing temperatures of water–urea mixtures depend on urea concentration. It can be noted that the

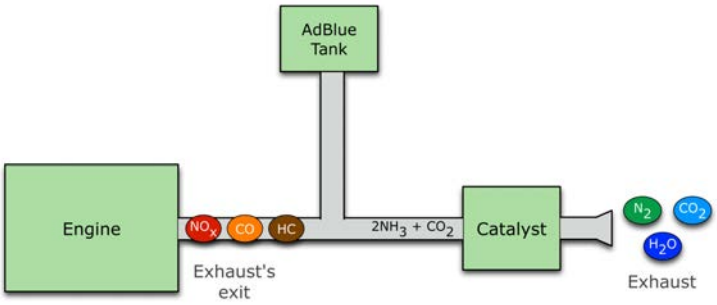

Figure 3.1: Basic scheme of the selective catalysis reduction system.

lowest freezing temperature (i.e. $-11\,°C$) corresponds to a mixture with a concentration of $32.5\,\%w/w$ of urea, which is the concentration of urea present in AdBlue®. In order to deal with a possible freezing of the catalyst, the containing tank is placed near the exhaust muzzle and maintained over the freezing point using a heating coil system.

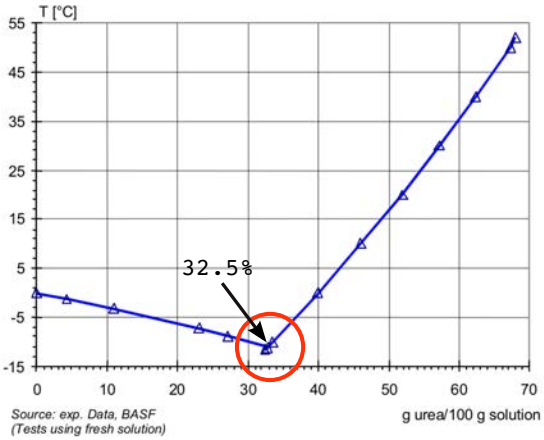

Figure 3.2: Freezing temperature of water–urea solutions with respect to urea concentration of the solution.

There are other problems related to the use of AdBlue® in addition to its freezing temperature:

- the possible refill of the tank with a liquid other than AdBlue®, such as diesel or water, which can result in a malfunction of the system, in an increase of unburned substances and in damages to the AdBlue® injection apparatus;
- the evaporation rates of water and urea are different, which leads to a spontaneous degradation of the mixture in time, reducing the efficiency of the

NO_x catalysis.

The proposed solution to overcome both these problems consists in adding an AdBlue® quality sensor, stopping the vehicle if the liquid contained in the tank does not meet the required properties.

The proposed sensor should have a set of features which allow it to be integrated into products developed by Röchling, in particular:

Simple and durable AdBlue® can be aggressive towards some materials due to its content of urea. The sensor should be in contact with AdBlue during the whole lifetime of the car, so it is important to choose an opportune material for the sensor;

Cheap the cost of the sensor should not affect significantly the price of the whole catalysis system;

Non-selective it should recognize variations of both the concentration of the water-urea mixture and the presence of different liquids (e.g. diesel, cola);

In-line the probe of the sensor should be placed in the tube connecting the tank to the exhaust system and measure the urea content in the liquid (i.e. AdBlue®) flowing into it.

The development of the proposed sensor was split into three phases:

1. Theoretical evaluation of all the possible physical properties that can be used to detect an anomaly in the AdBlue® solution. The results of the evaluation are reported in section 3.2.

2. Investigation of the electrical properties of the mixture, focusing on impedance and resistance. During this phase two sensor prototypes have been developed and characterised: an electrolytic sensor, presented in section 3.3, and a second sensor, protected by a non disclosure agreement.

3. Implementation of an embedded device capable of performing impedance and temperature measurements, improving the second sensor developed. This device is presented in section 3.5.

3.2 Possible approaches

Different exploitable physical properties were considered for the development of the sensor. The choice of the most suitable property was taken according to the analysis of already available sensors and by evaluating the feasibility of building a sensor, based on such property, with the required accuracy and realistically integrable into a vehicle.

In this section we will present the some of the different physical properties already exploited to track the concentration of urea in water, which are:

- Optical properties

- Viscosity
- Surface tension
- Thermal properties
- pH
- Electrical properties

3.2.1 Optical properties

Sensors exploiting optical properties are already available on the market, as the *Integrated AdBlue® Tank Level, Heating, Temperature and Quality Sensor* produced by Measurement Specialities (Figure 3.3). As the name suggests, these sensors are placed in the AdBlue® tank. The sensor has a working temperature between −40 °C and 125 °C and provides reliable measurements between −11 °C and 70 °C. The sensor can detect the presence of unwanted liquids (e.g. diesel, cola), allowing to stop the system before incidents.

Figure 3.3: Two examples of Measurement Specialities [4] optical sensors: (left) *QLS3851PL In-tank Quality & Level* and (right) *FPS6854 In-tank UQS*.

The sensor relies on optical spectrometric NIR technology to determine the urea percentage in the solution, allowing also to determine the presence of undesired substances.

One of the problems of this sensor is its accuracy, limited to ±2 % at all temperatures. Another problem is that optical sensors are placed in-tank, they are subject to local density and temperature fluctuations. The sensor can be affected by errors generated by dirt that can deposit on the measuring sensor's window, which alter the optical properties of the apparatus.

3.2.2 Viscosity

Measurement Specialities [4] also produces an AdBlue® quality sensor based on viscosity measurements, called *in-line urea quality sensor - Fluid Property Sensor*.

Measuring the frequency response of the fluid, this type of sensors is able to simultaneously measure viscosity, density, dielectric constant and temperature of a liquid. As the name suggests, it is an in-line sensor, thus allowing to control the quality of AdBlue®. This approach is better than placing an in-tank sensor as it excludes the possibility of contamination or degradation of the solution between the location of the analysis and the location of the catalysis.

The Fluid Property Sensor guarantees a precision of $\pm 1\,\%$ on the urea content and of $\pm 1\,^{\circ}\mathrm{C}$ on the temperature in the working range. Furthermore, it is capable of determining the presence of unwanted liquids in the system which could damage the catalysis system.

While this sensor satisfies most of the requests its lifetime is too short with respect to the whole life of a common car.

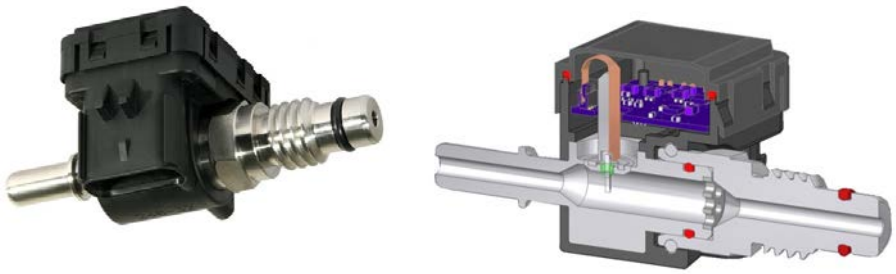

Figure 3.4: An example of inline viscosity sensors, *FPS5851HP In-line UQS*. This sensors is produced by Measurement Specialities [4].

3.2.3 Surface tension

Another possible approach is to analyse the surface tension of a liquid, in particular to estimate the surface tension fluctuations as a function of the urea percentage in the solution, exploiting capillarity, allowing the sensor to determine the composition of the fluid by analysing how it behaves in the capillaries.

It was however deemed hardly feasible adding a capillary in the AdBlue® line, especially due to the difficulty of emptying it after each measurement. This was likely the reason because no sensor based on this concept was found. The main reason for rejection of this sensor was a too small difference if surface tension between water and AdBlue® at $20\,^{\circ}\mathrm{C}$, measured respectively $72.8 \cdot 10^{-3}\frac{N}{m}$ and $65 \cdot 10^{-3}\frac{N}{m}$.

3.2.4 Thermal properties

There is no sensor currently on the market which exploits thermal properties to track AdBlue® quality. One of the possible approaches is to measure the specific heat of the liquid, but it was not considered as feasible as it would require a apparatus too invasive in order to create the necessary thermal isolation in a

plant exposed to motor thermal cycles and external temperature, which can differ greatly in few hours of operation.

3.2.5 Electrical properties

Equipment required to measure electrical quantities of fluids is easily integrable in a vehicle, as it is little enough and with low energy requirements. Furthermore, measurement of electrical properties is generally non invasive and has been already exploited with good results for the analysis of fluid in tree trunks.

Given these advantages given by the measurement of electrical properties both our team and Röchling decided to investigate this approach. A new sensors using the resistivity characteristics was developed.

3.3 Electrolytic sensor

The electrolytic sensor is based on one of the simplest type of electrical measurement (i.e. the specific resistance of the liquid), which allows to identify different water-urea mixtures. In order to perform such measurements a rough electrolytic cell was developed and characterized during IPSP2014.

3.3.1 Electrolytic cell

An electrolytic sensor 3.5 is comprised of a voltage generator, an ammeter and a voltmeter. The unknown resistance R (represented on the left of Figure 3.5) was a hand-built electrolytic cell (represented on the right of Figure 3.5) developed specifically for the application during IPSP2014.

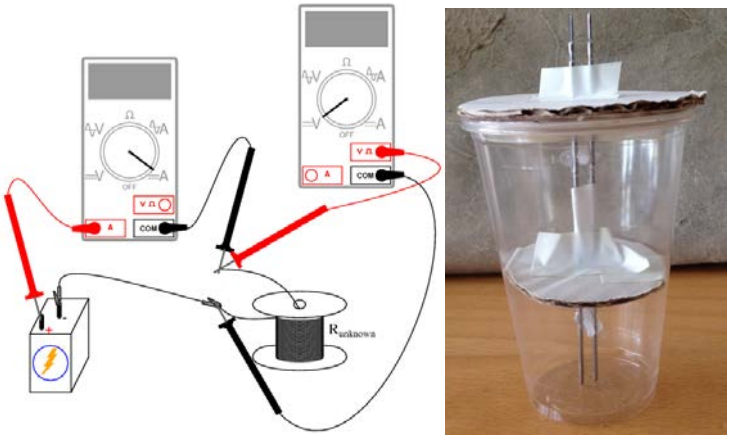

Figure 3.5: Left: generic apparatus to measure an unknown resistance. Right: picture of the hand-built electrolytic cell used during IPSP 2014.

The electrolytic cell developed during IPSP2014 consists of an electrode couple and a plastic container filled with a fixed quantity (57 mL) of the solution to

measure. The electrodes are two stainless steel cylinders with a diameter $\phi = 1.6\,\text{mm}$, maintained at a constant distance of $d = 3.6\,\text{mm}$ by two plastic dividers. In order to keep the surface of the cylinders immersed in the liquid constant a cardboard structure was designed to fix the position of the cylinders at the centre of the cell, allowing the same electrode couple to be used in different solution samples.

3.3.2 Main properties

Electrolytic sensors present a main problem: solution electrolysis, causing the electrical conductivity of the analysed mixture to change. This phenomenon leads to wrong measures, making it important to choose a voltage range such that the maximum applied voltages lead to negligible electrolysis (i.e. $1.2\,\text{V}$). Another typical problem of electrolytic cells is the oxidation of portion of the electrodes immersed in the solution, leading to a degradation of the quality of measurements. Lastly, the conductivity of a solution depends on the temperature of the solution itself, making it necessary to maintain the cell at a known temperature in order to obtain consistent data throughout its usage.

Resistance sensors, however, present most of the requirements listed in the introduction:

non-selective both water-urea solutions at different concentrations and liquids different from one another exhibit specific resistance values, allowing to distinguish them;

in-line it is possible to perform a resistance measurement in the liquid while it flows between the electrodes;

low-cost and simple thanks to both the materials used and its form the development and production costs of the proposed sensor are very low;

easily replaceable it is possible to integrate this device in a junction so that it can be replaced in case of degradation;

durable the use of stainless steel guarantees a long lifetime of the electrode, despite the corrosion by urea.

3.3.3 Time stability

As the sensor is required to work at least between two consecutive oil changes the first property to test is the robustness of the electrodes over time. In order to test this property an electrolytic cell was filled with pure AdBlue®, and maintained in a thermal bath (i.e. submerged in water and ice) for 18 consecutive hours, while applying a voltage swipe between $0\,\text{V}$ and $1.1\,\text{V}$ to the electrodes at steps of $0.02\,\text{V}$. Both the current value and the temperature of the thermal bath in which the solution was immersed were acquired for each voltage of the sweep.

The 3D plot in Figure 3.6 shows current versus temperature and applied voltage. The I-V characteristics of the solution were extrapolated for the various temperatures (shown on the right side of Figure 3.6), showing a correlation

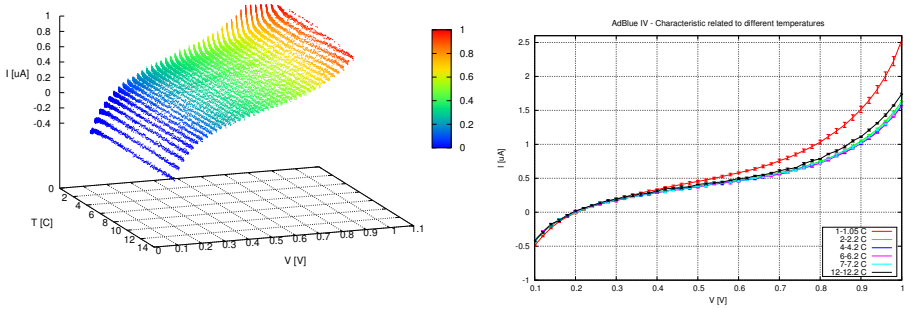

Figure 3.6: Left: measured current values versus temperature values and voltage applied to the electrolytic cell. Right: I-V characteristics of pure AdBlue® for different temperatures.

between temperature an I-V characteristics. While this result shows that it is possible to measure I-V characteristics at different temperatures, it also means that to run efficient AdBlue® quality measurements it is necessary to construct a calibration curve based on the final probe.

3.3.4 Measurement selectivity

Using a sensor similar to the previous one, tests have been performed to verify its accuracy in measuring the concentration of urea in water and in discriminating the presence of unwanted liquids. The test was ran by preparing 8 electrolytic cells with the same quantity (57 mL) of different liquids at room temperature: water, cola and six water-urea solutions at a concentration of either 20 %, 25 %, 31 %, 31.5 %, 32 %, 32.5 %w/w. Ten voltage swipes ranging from 0 V to 2 V at steps of 0.02 V were performed for each cell in order to construct an I-V calibration curve for each liquid (reported in Figure 3.7). As can be noted from the calibration curves, it is possible to discriminate between the different liquids. In order to estimate the sensitivity of the proposed sensor in discriminating the liquids the development focused on four voltages: 0.6, 1.0, 1.2 and 1.6 V (the I-V characteristics for each specific voltage have been reported in Figure 3.8).

At 0.6 V the calibration curve shows a distinct difference in current between cola, water, the 32.5 %w/w water-urea mixture and the 32 %w/w mixture, but the remaining mixtures are overlapped. At 1.0 V, instead, the currents corresponding to the eight solutions are separated from each other by at least two standard deviation. However it was deemed as more robust to have a calibration curve with a stronger distinction between the various solutions. At 1.2 V, water-urea solutions are easier to distinguish, while the differences between water and cola are smaller, making them harder to recognise. At 1.6 V not only the voltage is in the range of non-negligible hydrolisis, but the differences in current between the various solutions are too small to be distinguished, making it an unsuitable voltage for quality sensing.

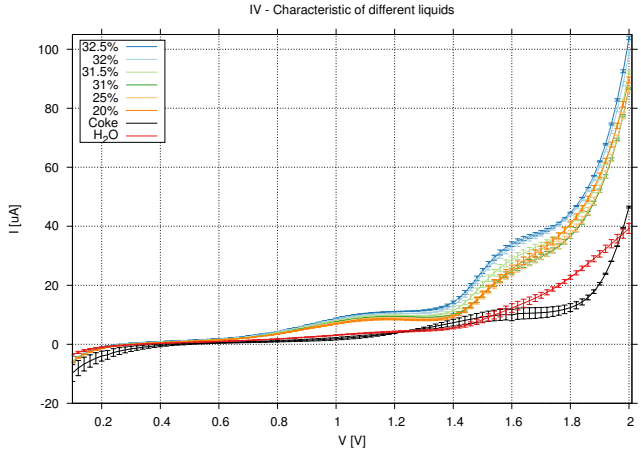

Figure 3.7: I-V characteristics of water, cola and six water-urea solutions at a concentration of either 20 %, 25 %, 31 %, 31.5 %, 32 %, 32.5 %w/w at room temperature.

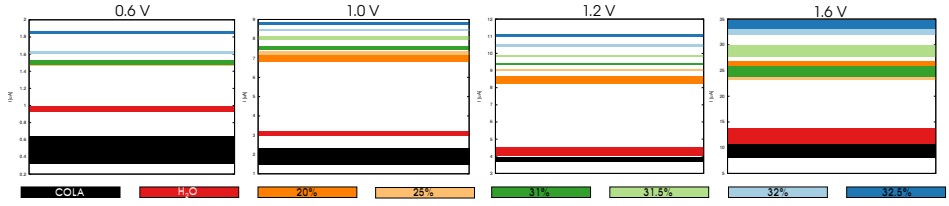

Figure 3.8: Details of the I-V characteristics shown in Figure 3.7 in the neighborhood of four different voltage values: 0.6, 1.0, 1.2 and 1.6 V.

3.3.5 Calibration curve

Given the previous results the operating voltage chosen for the electrolytic sensor was 1.2 V. The distance between the two steel cylinders was decreased in order to increase the signal amplitude read by the sensor. Due to both of these reasons it was necessary to construct an additional calibration curve based on the new probe. The calibration was designed to acquire the current for each liquid (i.e. water, cola, water-urea mixtures with different urea concentrations) for 9 consecutive minutes. During the first minute of the measurement a large variation of the current was observed, probably due to the stabilization of the probe. For this reason the first minute was not considered in data post-processing.

The time series of the current for each concentration of urea are shown in Figure 3.9 on the left, exhibiting a correlation beween current and three different concentration values, specifically 32.5 %, 32 % and 31.5 %w/w.

The distributions of the measured values were calculated for each solution, in order to understand how the current distributed with respect to the concentration, and were then fitted using a Gaussian function. The Gaussian distributions related to the concentrations of the urea in water are shown in Figure 3.9 (right). As can be noted the distribution related to AdBlue® is separated from the other

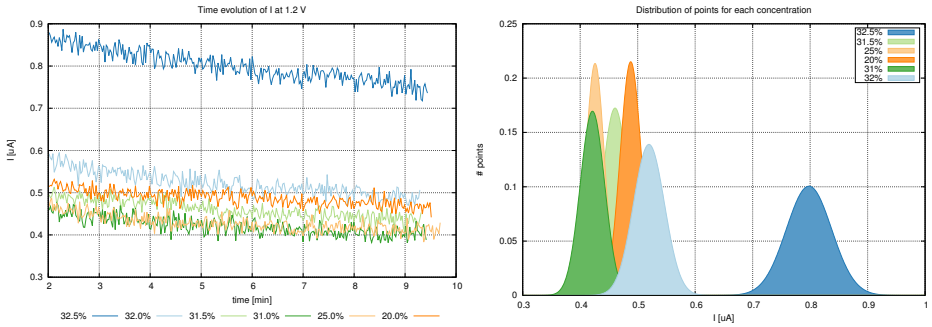

Figure 3.9: Left: Current value versus time for 32.5 %, 32 %, 31.5 %, 31 %, 25 % and 20 % w/w concentrated water-urea solutions. Right: Gaussian distributions of current values for the water-urea solutions taken into account.

distributions, which are instead partially overlapping. Using both the mean value and the standard deviation of each concentration distribution it was possible to construct a calibration curve, presented in Figure 3.10.

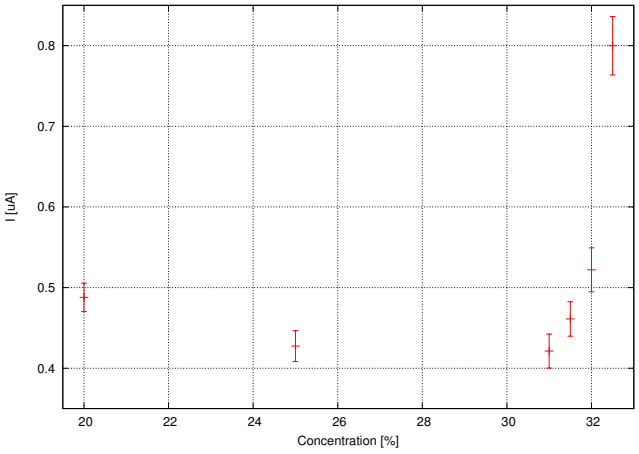

Figure 3.10: Current versus concentration of urea in water $w/w\%$. The error bars are given by the standard deviation.

The calibration curve shows that each concentration corresponds to a different current value, allowing the sensor sensor to meet the requirements requested by Röchling.

3.4 The second sensor

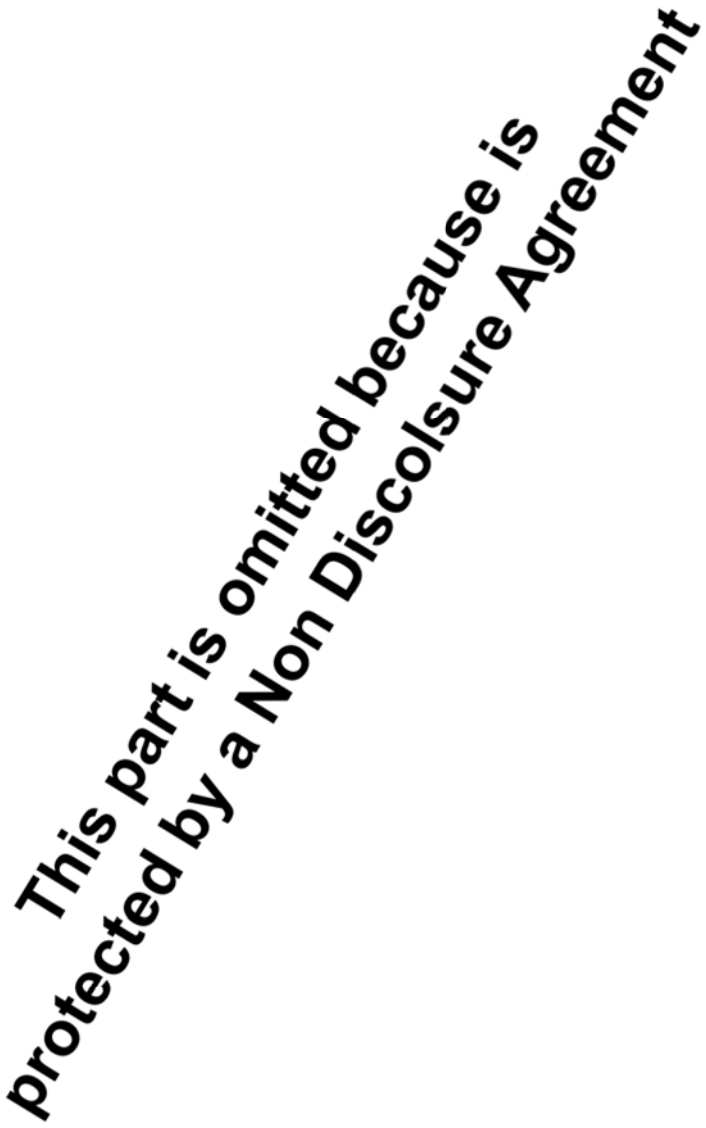

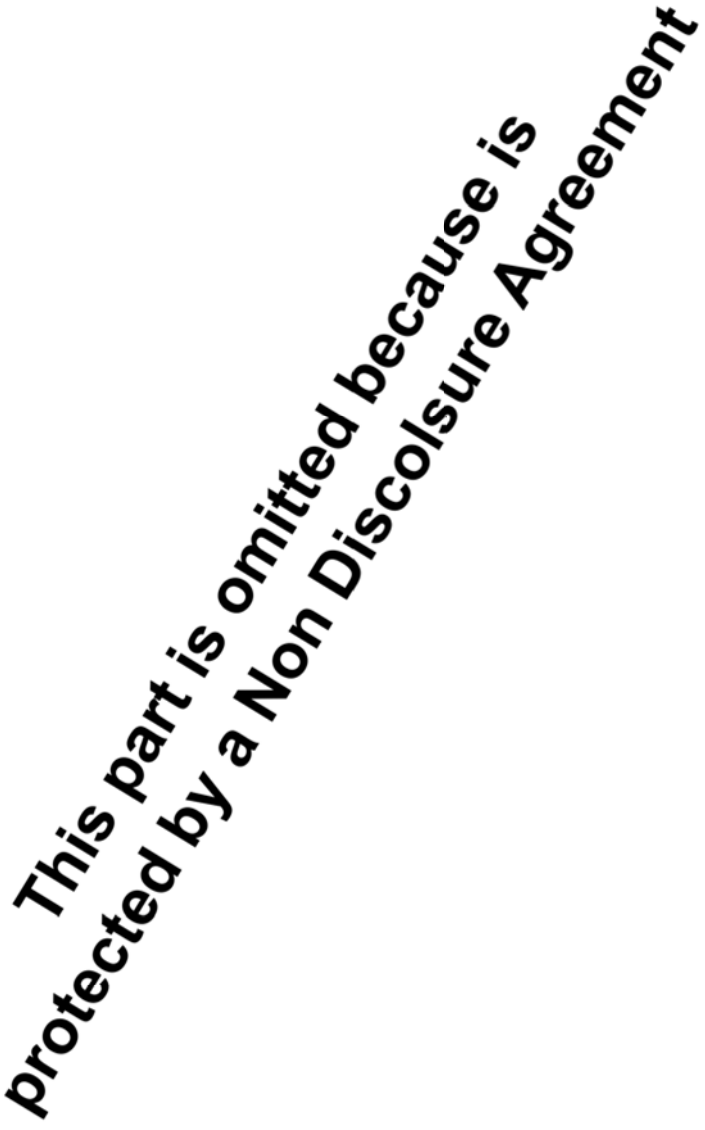
This part is omitted because is
protected by a Non Disclosure Agreement

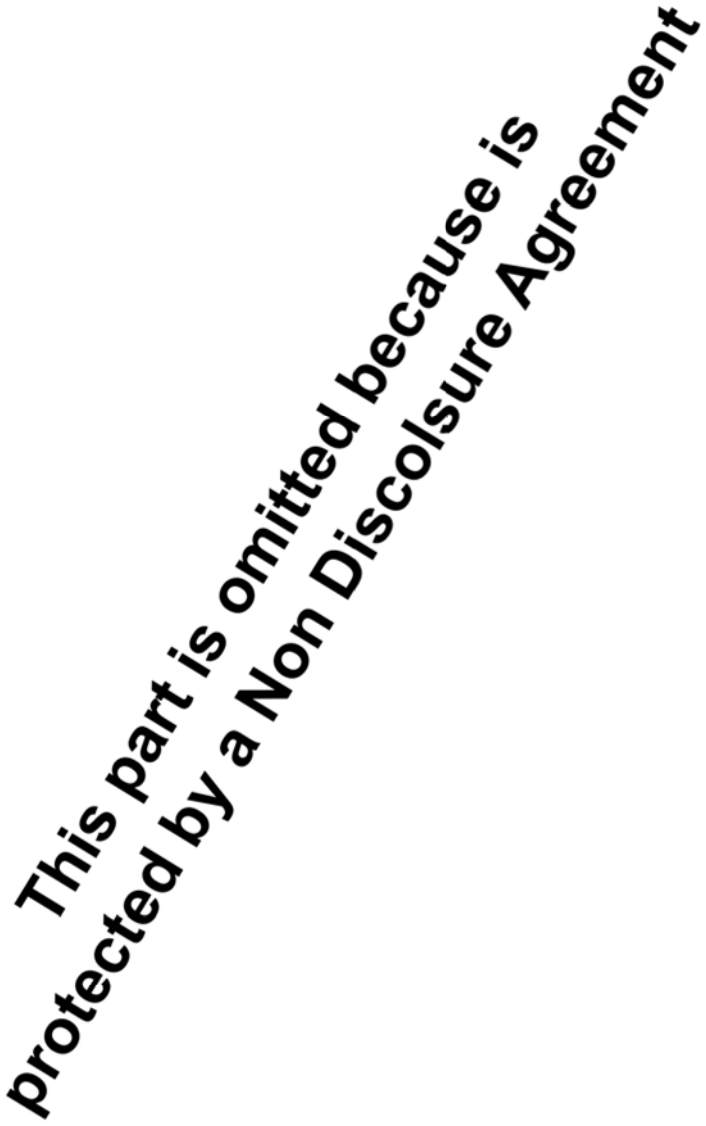
This part is omitted because is
protected by a Non Discolsure Agreement

3.5 Prototype of an embedded measurement system

During IPSP 2014, an embedded electronic device was also developed in order to acquire data by using the sensors of sections 3.3.

The developed device employs an AD5933[5], produced by *Analog Devices*, a high precision impedance converter system that combines an on-board frequency generator with a 12-bit, 1 MSPS, analog-to-digital converter (ADC). AD5933's outputs are on-board temperature and the impedance spectrum of a connected network. Using the impedance it is possible to compute the resistance values of the connected networks (e.g. an electronic circuit). This computation has been done using a BeagleBone board[6], connected to an AD5933 using the I2C protocol[7]. The BeagleBone is a credit-card-sized prototyping board that can run Linux and is provided with an ethernet interface allowing for rapid development through SSH. The BeagleBone is a cheap solution for embedded development as it provides developers with an array of both ADCs and GPIO headers, along with a relatively fast ARM processor and a dedicated Ubuntu version, which makes use of the hardware floating point processors.

In order to provide a viable solution in automotive applications we started working on a C project to track the variation in AdBlue® density using the method shown in 3.3, managing to interface the prototyping board to an AD5933 and run various probing tests in order to calibrate the sensor. Due to a number of problems in setting up the environment, however, it was not possible to complete all the necessary tests to complete the calibration, but provided with the results of the experimental tests it would be a matter of implementing an algorithm to periodically run a network analysis using the AD5933 to track any change in the AdBlue® contentration.

3.6 Conclusions and future development

During IPSP2014, two sensors have been developed to measure the urea concentration in the tube between the tank and the exhaust pipe. Additionally an embedded system has been developed to perform in-line quality measurement of AdBlue®.

The resistive sensor is characterized by its simplicity, a low price and versatility, satisfying Röchling's requests: in-line with an accuracy of $\approx 0.2\%$. A way to improve this sensor is to use Bayesian machine learning methods and to change the electrodes geometry. The second sensor needs additional work to be integrated on an automotive system.

Bibliography

[1] European parliament. Regulation (ec) no 715/2007. `http://goo.gl/XsEKm1`, June 2007.

[2] Wikipedia.org. European emission standards. `http://goo.gl/7gjOF8`.

[3] BASF. Adblue technical leaflet. `http://goo.gl/ljfdVj`, November 2006.

[4] Measurement Specialties Inc. Improvements in scr systems enabled by urea quality sensing. `http://www.meas-spec.com/`, June 2013.

[5] Analog Devices. Ad5933: Product details. `http://goo.gl/1vZI61`.

[6] BeagleBoard.org. Beaglebone. `http://beagleboard.org/bone`.

[7] Wikipedia.org. I2c. `http://goo.gl/5Rhscu`.

CHAPTER
FOUR

CREDITS

Adige BLM Group S.p.A.

From left to right, upper row: Mattia Mancinelli[1]; Alessandro Toffali[1]; Martino Bernard[1]; Luca Matteo Martini[1,2]; Alessandro Trenti[1].

From left to right, lower row: Massimo Echer[1]; Marco Scapinello[3]; Simone Donadello[1].

Not in figure: Claudio Castellan[1].

[1] Department of Physics, University of Trento, via Sommarive 14, I-38123 Povo (Trento), Italy
[2]The IPSP2014 organisation committee
[3] CNR-IMCB, U.O.S. Trento, via Sommarive 14, I-38123 Povo (Trento), Italy


IPSP2014
INDUSTRIAL
PROBLEM SOLVING
WITH PHYSICS

Aquafil S.p.A.

From left to right, upper row: Elia Schneider[1]; Faraz Deirmina[2]; Alessio Caciagli[3]; Davide Gandolfi[1,4]; Filippo Benetti[5]; Giovanni Giusti[6]; Claudio Nidasio[7].

From left to right, lower row: D.M.S. Sultan[2]; Stefano Tondini[1,8]; Natascia Cozza[5].

[1] Department of Physics, University of Trento, via Sommarive 14, I-38123 Povo (Trento), Italy
[2] Department of Industrial Engineering, University of Trento, via Sommarive 9, I-38123 Povo (Trento), Italy
[3] Debye Institute for Nanomaterials Science, Utrecht University, Padualaan 8, 3584 CH Utrecht, The Netherlands
[4] The IPSP2014 organisation committee
[5] Department of Industrial Engineering and Biotech Center, University of Trento, via delle Regole 101, I-38123 Mattarello (Trento), Italy
[6] Istituto dei Materiali per l'Elettronica ed il Magnetismo - CNR - sede di Trento, via alla Cascata 56/C, I-38123 Povo (Trento), Italy
[7] Technology Transfer Support Division, University of Trento, via Calepina 14, I-38122 Trento, Italy
[8] Physics and Nanoscience School of Graduate Studies, University of Modena and Reggio Emilia, Modena, Italy


Energy balance
Rate approach
IPSP2014
INDUSTRIAL
PROBLEM SOLVING
WITH PHYSICS

Röchling Automotive SE&Co.KG

From left to right, upper row: Michele Bianchi[1]; Marta Guarisco[2]; Nicola Cagol[3]; Zahra Bisadi[2]; Michele Valentini[2].

From left to right, lower row: Stefano Bacchi[2]; Marika Falciano[2]; Matteo Franchi[2,4]; Marco Vardaro[2].

[1] Department of Information Engineering and Computer Science, University of Trento, via Sommarive 9, I-38123 Povo (Trento), Italy

[2] Department of Physics, University of Trento, via Sommarive 14, I-38123 Povo (Trento), Italy

[3]Department of Industrial Engineering and Biotech Center, University of Trento, via delle Regole 101, I-38123 Mattarello (Trento), Italy

[4]The IPSP2014 organisation committee

ACKNOWLEDGEMENT

We acknowledge the Department of Physics, the Research and Technology Transfer Support of the University of Trento and Confindustria Trento. We are particularly grateful to Adige BLM Group S.p.A., Aquafil S.p.A. and Röchling Automotive SE&Co.KG for the enthusiasm and the support they gave us during the IPSP2014 week, and to all the students/researchers that had been working hard during the event week. We would like to thank IPSP2014 sponsors: Gambetti Kenologia, MUSE Museo delle Scienze, I.R.S. - National Instruments and Famiglia Cooperativa di Povo for the financial and material support.

IPSP2014 could not have been organised without the help of the staff of Comunicazione Polo collina of University of Trento, and of the Graphic Service of the University of Trento. In particular we would like to express our special thanks to Lucia Dorna. We acknowledge the IPSP2014 Advisory Board and in particular Vanessa Ravagni for her helpful advice. We also would like to thank the staff of the Laboratori Didattici, Department of Physics of University of Trento, who made available their instrumentation and laboratories.

Finally a special thank to our wives and girlfriends, and to all the people who believed in our project and supported us during the organisation of IPSP2014.

Matteo Franchi
Davide Gandolfi
Luca Matteo Martini
Scientific Committee of Industrial Problem Solving with Physics 2014

ART>UNITRENTO
January 2015

Industrial Problem Solving with Physics (IPSP2014) is a one-week event organized by the Department of Physics and the Research and Technology Transfer Support Division of the University of Trento, in collaboration with Confindustria Trento.

3 companies and 30 brains (master course students, PhD students and fellow researchers) were selected and worked together to find solutions to practical industrial problems proposed by the participating companies.

Young and motivated researchers had the chance to show off their skills in tackling new practical challenges. The participating companies obtained solutions to their problems and experience an alternative problem solving strategy.

http://events.unitn.it/en/ipsp2014

Participant companies

BLM GROUP ADIGE

AQUAFIL synthetic fibres and polymers

RÖCHLING Automotive

Sponsors

Gambetti Vacuum Technology and Related Solutions

Museo delle Scienze MUSE

NATIONAL INSTRUMENTS

POVO FAMIGLIA COOPERATIVA coop

ISBN 978-88-8443-581-1